Force–Field–Based Computational Study of the Thermodynamics of a Large Set of Aqueous Alkanolamine Solvents for Post–Combustion CO_2 Capture

Javad Noroozi[†] and William R. Smith[*,‡,¶]

†*Department of Chemical Engineering, University of Waterloo, Waterloo ON N2L 3G1, Canada*

‡*Department of Mathematics and Statistics, University of Guelph, Guelph ON N1G 2W1, Canada*

¶*Faculty of Science, Ontario Tech University, Oshawa ON L1H 7K4, Canada*

E-mail: bilsmith@uoguelph.ca

Abstract

The ability to predict the thermodynamic properties of amine species in CO_2-loaded aqueous solutions, including their deprotonation (pK_a) and carbamate to bicarbonate reversion (pK_c) equilibrium constants and their corresponding standard reaction enthalpies, is of critical importance for the design of improved carbon capture solvents. In this study, we used isocoulombic forms of both reactions to determine these quantities for a large set of aqueous alkanolamine solvent systems. Our hybrid approach involves using classical molecular dynamics simulations with the General Amber Force Field (GAFF) and semi–empirical AM1–BCC charges (GAFF/AM1–BCC) in the solution phase, combined with high level composite quantum chemical ideal-gas calculations.

We first determined a new force–field (FF) for the hydronium ion (H_3O^+) by matching to the single experimental (pK_a) data point for the well–known MEA system at 298.15 K. We then used this FF to predict the pK_a values for 76 other amines at 298.15 K and for all 77 amines at elevated temperatures. Additionally, we indirectly relate the H_3O^+ hydration free energy to that of H^+, and provide expressions for intrinsic hydration free energy and enthalpy of the proton.

Using the derived H_3O^+ FF, we predicted the (pK_a) values of a diverse set of alkanolamines with an overall AAD of less than 0.72 pK_a units. Furthermore, the derived H_3O^+ force field is able to predict the protonation enthalpy of these amines when used with the GAFF. We also predicted the carbamate reversion constants of the primary and secondary amine species in the data set and their corresponding standard heats of reaction, which we compared with the scarcely available experimental data, which are often subject to significant uncertainty. Finally, we also described the influence of electronic and steric of different molecular fragments/groups on the stabilities of the carbamates.

1 Introduction

The combined absorption–stripping process using aqueous amine solvents is considered to be the dominant near–term technology for large–scale CO_2 capture from point sources, such as coal-fired power plants, and cement and steel plants.[1] CO_2 is primarily absorbed in the form of carbamate and bicarbonate ions, and stripped off in a later stage of the process by supplying heat to reverse the reaction and release the absorbed CO_2.[2]

There is continuing interest in discovering CO_2 solvents that show improvements over the traditional monoethanolamine (MEA) base case, and the solvent's equilibrium CO_2 solubility is a property of primary importance. This is governed by the equilibrium constants and their temperature dependence for the involved underlying reactions, which may be represented by

the following set:

$$\mathrm{RNH_3^+ + H_2O} = \mathrm{RNH_2 + H_3O^+} \quad \text{(R1)}$$

$$\mathrm{RNHCO_2^- + H_2O} = \mathrm{RNH_2 + HCO_3^-} \quad \text{(R2)}$$

$$\mathrm{CO_2 + 2H_2O} = \mathrm{HCO_3^- + H_3O^+} \quad \text{(R3)}$$

$$\mathrm{H_2O + HCO_3^-} = \mathrm{CO_3^{-2} + H_3O^+} \quad \text{(R4)}$$

$$\mathrm{2H_2O} = \mathrm{H_3O^+ + OH^-} \quad \text{(R5)}$$

$$\mathrm{CO_2} = \mathrm{CO_2(vap)} \quad \text{(R6)}$$

All species are in the aqueous solution phase unless indicated otherwise, and $\mathrm{RNH_2}$, $\mathrm{RNH_3^+}$ and $\mathrm{RNHCO_2^-}$ denote the neutral, protonated and carbamate forms of the amine solvent respectively. Tertiary amines do not form carbamates, resulting in the omission of reaction R2 for these compounds.

A main concern associated with the $\mathrm{CO_2}$ capture process is the high energy demand for solvent regeneration, due to the relatively stable $\mathrm{CO_2}$-containing solution species, coupled with the high latent heat of the water co-solvent. This is particularly acute for primary amines, which tend to form more stable carbamates than is the case for secondary and sterically hindered amines, but they have the advantage of exhibiting faster reaction kinetics than the latter group of compounds.[3] On the other hand, tertiary amines have the advantage that $\mathrm{CO_2}$ reacts in an overall 1:1 stoichiometric ratio with respect to the amine solvent (the combination $\mathrm{R3 - R1}$ of the above reaction set), whereas primary and secondary amines react in only an overall 1:2 stoichiometric ratio (the combination $\mathrm{R3 - R1 - R2}$). However, this advantage of tertiary amines is offset by their slower reaction kinetics.

The equilibrium constants (expressed in terms of their $\mathrm{p}K$ values) are commonly obtained experimentally from concentration measurements in relatively dilute equilibrium solutions or by their extrapolation to zero ionic strength, typically in conjunction with a Debye-Hückel-related equation to model the species activity coefficients.[4–6] Whereas the $\mathrm{p}K_a$ of the amine

deprotonation reaction R1 can be measured relatively accurately by means of potentiometric titration or by spectroscopic concentration measurements in a CO_2-free solution,[7,8] accurate determination of pK_c for the carbamate reversion reaction R2 is more challenging[9] due to the presence in a CO_2-loaded solution of the coexisting species involved in the indicated set of reactions. In addition, due to the rapid proton exchange, NMR techniques cannot distinguish between the bicarbonate/carbonate species peaks or the amine/protonated amine species peaks, and only the sums of the relevant individual species concentrations in each pair can be determined. This has resulted in the use of different approaches to unravel the individual species concentrations from the NMR data.[10–12] By relating the intensity of the two–species compound peak to the individual species peaks and their concentrations in the solution, amine and its protonated form may be distinguished by interpolation of the NMR chemical shifts at low and high pH values or by measuring the spectra of solutions that contain only the individual species.[11] In addition, species at concentrations less than about 10^{-4} molal are undetectable by the analysis of NMR data. These experimental challenges typically result in a significant uncertainty in the resulting carbamate reversion constant values, even for the well–studied monoethanolamine (MEA)[9] system.

A common theoretical approach to determine pK values uses ideal-gas electronic structure (ES) calculations in conjunction with conductor–like polarizable continuum models (CPCM), universal solvation models (SMD, SM8), or their explicit solvent variants (the inclusion of explicit solvent molecules in the first solvation shell).[13,14] The calculation of solvation free energy using such models requires five temperature–dependent solvent–based parameters based on experimental data: dielectric constant, bulk surface tension, refractive index, and acidity and basicity parameters. The accuracy of these models is often unsatisfactory, in part because their development and application has generally been limited to small rigid molecules; furthermore, the models have only been parameterized at 298.15 K. Their static nature also hampers extensions to flexible molecules in solution, in which the contribution of different molecular conformers to the solvation free energy is non-negligible. In a notable

study, Coote *et al.*[15] demonstrated different criteria for obtaining the most stable conformer in the solution phase, and showed how an erroneous result may be obtained if the commonly used gas–phase geometry is adopted for the solution phase solvation free energy calculation in the case of larger flexible amine molecules.

Since the pioneering study of da Silva and Svendsen,[16] numerous studies have used a similar thermodynamic-cycle-based approach[17] to investigate the deprotonation reaction pK_a value, whereas similar studies for the carbamate reversion equilibrium constant pK_c are extremely limited.[16] While some studies show reasonable accuracy (a mean absolute deviation from experiment below 0.5 pK unit), they usually require a particular combination of gas–phase quantum chemical theory/basis set and solvation model that is often different from the original quantum chemical method used for the solvation model development, questioning the transferability of such approaches to different classes of compounds.[14,18]

More rigorous direct *ab initio* simulation of the free-energy profile of the dissociation reaction taking place in the condensed phase has been shown to be a promising route for pK_a estimation.[19] However, apart from being extremely computationally demanding, such simulations may require advanced sampling techniques to escape from local free energy minima, inhibiting their wide-spread use for rapid solvent screening.[20]

In a recent paper,[21] we developed a molecular–based framework for reactive absorption in CO_2-amine-water systems without any amine-specific experimental data or experimental proton hydration free energy data only using the pK_c and the equilibrium constant of the following *isoelectric* reaction (one with the same total numbers of positive and negative charges on the reactant and product side), which is the reaction combination R3-R1-R2 of the above reaction set:

$$\mathrm{RNH_2 + 2CO_2} \quad = \quad \mathrm{RNH_3^+ + RNHCO_2^-} \tag{R7}$$

We combined these equilibrium constants with a Henry-law-based thermodynamic model

and the experimentally well-known pK values for the binary CO_2-H_2O system to predict the speciation and other quantities of interest for a set of 7 CO_2–loaded primary and secondary alkanolamine solvents.

In this paper, we refine our methodology by focusing on the deprotonation reaction R1 and the carbamate reversion reaction R2, both of which are *isocoulombic* (with the same number of like-charged species on the reactant and the product side). Use of an isocoulombic reaction has been shown to provide a better estimate of the temperature trend for its equilibrium constant.[22] Furthermore, such reactions have the advantage that for activity coefficient models based on the Debye-Huckel approximation (*e.g.*, the Davies model), the ionic contributions to the reaction free energy change cancel. We test this approach for the equilibrium constants (pK_a and pK_c) for a much larger set of 77 primary, secondary and tertiary amines, Our approach combines ideal-gas calculations with explicit solvent MD simulations in TIP3P water using the fast AM1-BCC partial charge assignment method for the amine molecules and their protonated and carbamate forms, which we have previously shown to be superior to the RESP-based charges for pK_a prediction used in our previous work.[23]

To enable the use of the isocoulombic reaction R1, we develop a new GAFF-compatible force field for H_3O^+ to be used in conjunction with TIP3P water by matching the well—known experimental MEA deprotonation equilibrium constant at 298.15 K. This enables the H_3O^+ FF to be used to calculate the pK_a of reaction R1 as a function of temperature, both for MEA and all other alkanolamines. We further validate the H_3O^+ FF by comparing its indirect prediction of proton hydration free energy with the well-established literature value at 298.15 K,[24] and also use it to calculate the intrinsic proton solvation free energy as a function of temperature.

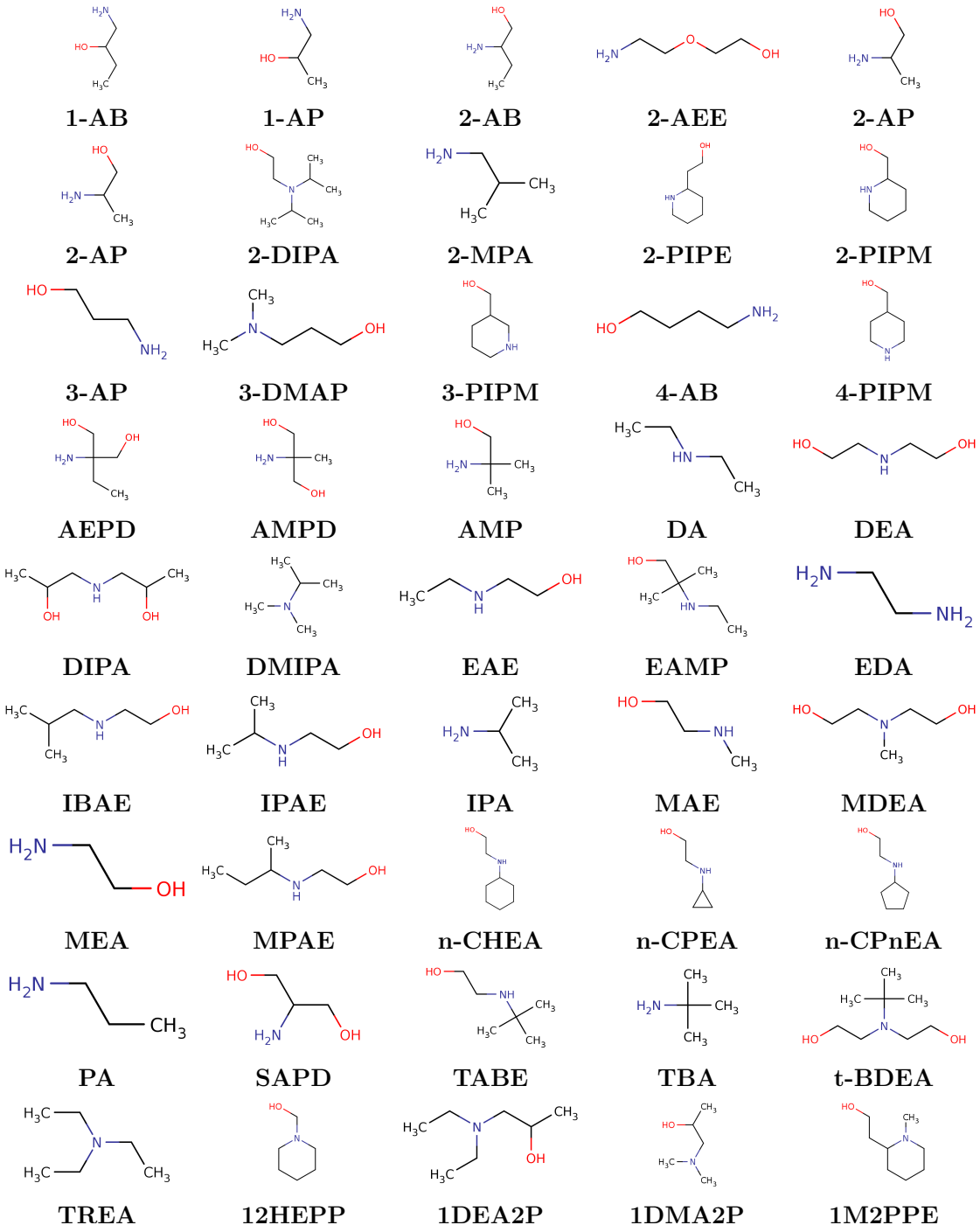

Figure 1: Molecular Structures of the alkanolamines considered in this work.

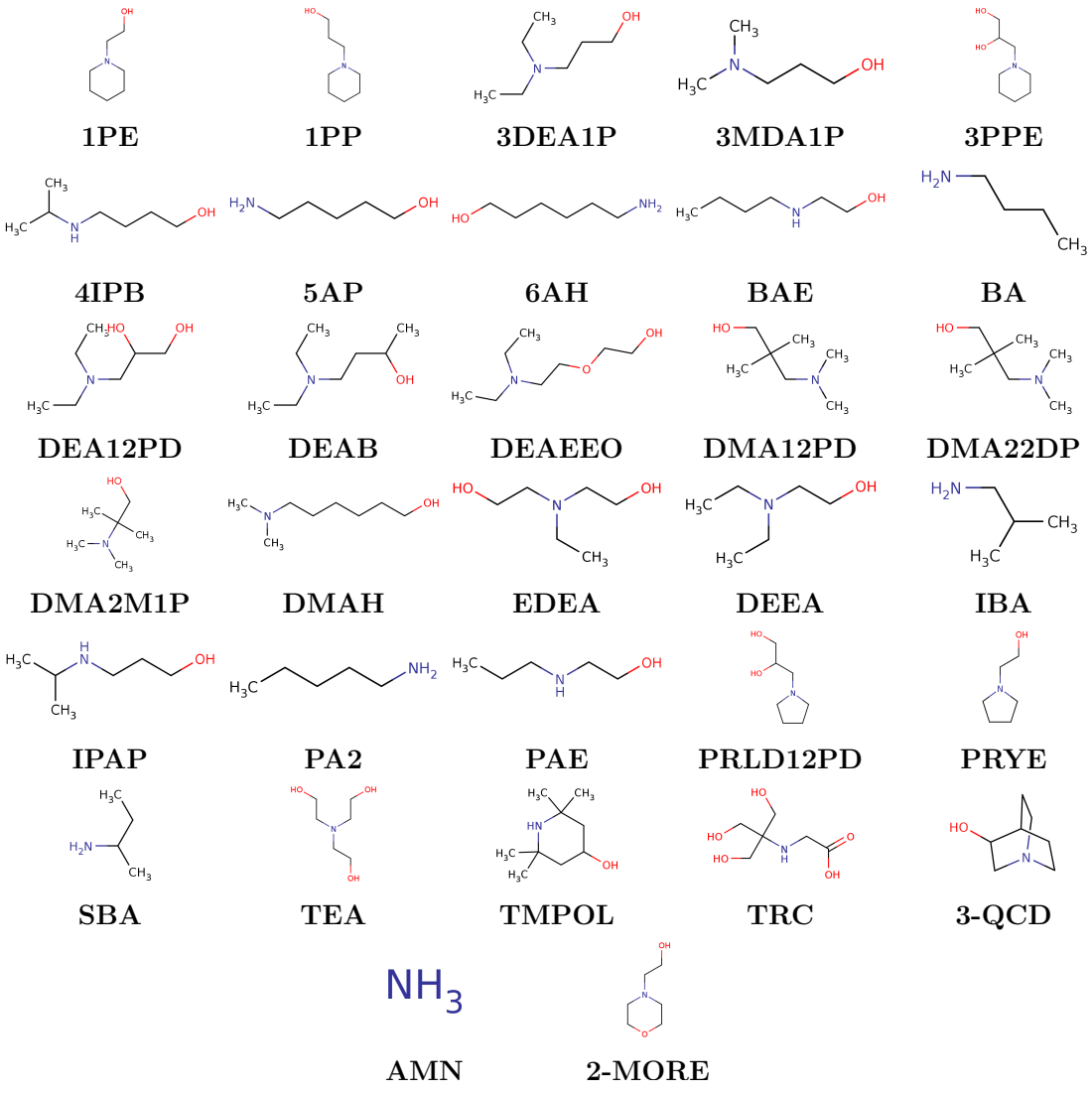

Figure 2: Molecular Structures of the alkanolamines considered in this work (continued).

2 Thermodynamic Background

2.1 Molecular–based framework for the calculation of pK_a and pK_c

Our framework for predicting pK_a and pK_c without the need for experimental data is described in detail in our previous papers,[21,23,25] and only a brief summary is provided here.

The species Henry-Law-based standard chemical potential using the molality concentration variable, $\mu_i^\dagger(T,P)$, may be defined for both solutes and the solvent, and is related to the infinite dilution *intrinsic solvation free energy* (self solvation free energy in the case of the solvent), $\mu_i^{\mathrm{res},NVT;\infty}[T,\rho(T,P)]$, by

$$\mu_i^\dagger(T,P) = \mu_i^0(T;P^0) + RT\ln\left(\frac{RT}{100P^0}\right) + RT\ln\left(\frac{\overline{\rho}_{\mathrm{solv}}(T,P)}{1000}\right) + \mu_i^{\mathrm{res},NVT;\infty}[T,\rho_{\mathrm{solv}}(T,P)] \tag{7}$$

where $\mu_i^0(T;P^0)$ is the species ideal–gas (IG) chemical potential at T and reference state pressure $P^0 = 1$ bar, P is expressed in bar, and ρ_{solv} is the density of the pure solvent. ($\overline{\rho}_{\mathrm{solv}}$ denotes its expression in kg m^{-3}). $\mu_i^\dagger(T,P)$ is numerically equal to the species chemical potential in a hypothetical ideal solution of unit molality.

The pK value for a reaction j is obtained from the concentration-independent quantity $\Delta G_j^*(T,P)$, via

$$pK_j(T,P) = \frac{\Delta G_j^*(T,P)}{RT\ln(10)} \tag{8}$$

where $\Delta G_j^*(T,P)$ is the standard Gibbs energy change of the reaction in the solvent, given by

$$\begin{aligned}
\Delta G_j^*(T,P) &= \sum_{i=1}^{N_s}\nu_{ij}\mu_i^\dagger(T;P) + RT\nu_{\mathrm{solv},j}\ln\left(\frac{1000}{M_{\mathrm{solv}}}\right) \\
&= \Delta G_j^0(T;P^0) + RT\overline{\nu}_j\ln\left(\frac{RT}{100P^0}\right) + RT\overline{\nu}_j\ln\left(\frac{\overline{\rho}_{\mathrm{solv}}(T,P)}{1000}\right) \\
&\quad + RT\nu_{\mathrm{solv},j}\ln\left(\frac{1000}{M_{\mathrm{solv}}}\right) + \Delta G^{\mathrm{res},NVT;\infty}(T,P)
\end{aligned} \tag{9}$$

where

$$\begin{aligned} \Delta G_j^0(T;P^0) &= \sum_{i=1}^{N_s} \nu_{ij}\mu_i^0(T;P^0) \\ \Delta G_j^{\mathrm{res},NVT;\infty}(T,P) &= \sum_{i=1}^{N_s} \nu_{i,j}\mu_i^{\mathrm{res},NVT;\infty}[T,\rho(T,P)] \end{aligned} \tag{10}$$

N_s is the number of species involved in the reaction, ν_{ij} is the stoichiometric coefficient of species i in reaction j (conventionally positive for products and negative for reactants), $\bar{\nu}_j = \sum_i \nu_{ij}$ and M_{solv} is the solvent (water in this case) molecular weight.

For the deprotonation and carbamate reversion reactions in this study (reactions R1 and R2, respectively, $\bar{\nu}_j = 0$ and $\nu_{\mathrm{solv},j} = -1$, and the following expression for ΔG_j^* is obtained for both reactions:

$$\Delta G_j^*(T,P) = \Delta G_j^0(T;P^0) + \Delta G^{\mathrm{res},NVT;\infty}[T,\rho(T,P)] - RT\ln\left(\frac{1000}{M_{\mathrm{solv}}}\right) \tag{11}$$

$$= \Delta G_j^\dagger(T,P) - RT\ln\left(\frac{1000}{M_{\mathrm{solv}}}\right) \tag{12}$$

Finally, the temperature dependence of pK for the deprotonation and carbamate reversion reactions is obtained by application of the Gibbs-Helmholtz equation to Eqs. (11) and (8), resulting in :

$$\begin{aligned} \left(-\frac{\partial \ln K_j}{\partial T}\right) = \left(\frac{\partial \Delta G^\dagger[T,P]/RT}{\partial T}\right) &= \frac{\partial(\Delta G_j^0[T;P]/RT)}{\partial T} + \frac{\partial(\Delta G^{\mathrm{res},NVT;\infty}/RT)}{\partial T} \\ &= -\frac{\Delta H^0(T,P)}{RT^2} - \frac{\Delta H^{\mathrm{res},NVT;\infty}[T,\rho(T,P)]}{RT^2} \\ &= -\frac{\Delta H^\dagger(T,P)}{RT^2} \end{aligned} \tag{13}$$

Assuming a linear temperature dependence of the enthalpy quantities in each term (equivalent to assuming constant reaction ΔC_p values) gives an expression at the pressure of interest

of the form

$$-\ln K_j = A_j^0 + \frac{B_j^0}{T} + C_j^0 \ln(T) + A_j^{\rm res} + \frac{B_j^{\rm res}}{T} + C_j^{\rm res} \ln(T) \tag{14}$$

2.2 H_3O^+ FF determination and the proton hydration free energy

Replacing H_3O^+ in reaction R1 by H^+ would yield the alternative reaction equation

$$\mathrm{RNH_3^+ = RNH_2 + H^+} \tag{R8}$$

The reaction combination R1-R8 gives the reaction

$$\mathrm{H_2O + H^+ = H_3O^+} \tag{R9}$$

Since by convention, in water solvent ΔG^* for reaction R5 and for the following reaction are identical:

$$\mathrm{H_2O \;\; = \;\; H^+ + OH^-} \tag{R10}$$

this means that ΔG^* for reaction R9=R5-R10 must vanish. Hence the pK values for reactions R1 and R8 must also be identical. Eqs. (8) and (9) for reaction R8 give

$$\begin{aligned} RT\ln(10) pK_{R8}(T,P) &= \Delta G^0_{R8}(T;P^0) + \mu_{\rm H^+}^{{\rm res},NVT;\infty}(T,P) + \mu_{\rm RNH_2}^{{\rm res},NVT;\infty}(T,P) - \mu_{\rm RNH_3^+}^{{\rm res},NVT;\infty}(T,P) \\ &\quad + RT\ln\left(\frac{\overline{\rho}_{\rm solv}(T,P)}{1000}\right) + RT\ln\left(\frac{RT}{100P^0}\right) \end{aligned} \tag{15}$$

The proton intrinsic hydration free energy, $\mu_{\rm H^+}^{{\rm res},NVT;\infty}$, is then given by

$$\begin{aligned} \mu_{\rm H^+}^{{\rm res},NVT;\infty}(T,P) &= RT\ln(10) pK_{R8}(T,P) - \Delta G^0_{R8}(T;P^0) - \mu_{\rm RNH_2}^{{\rm res},NVT;\infty}(T,P) + \mu_{\rm RNH_3^+}^{{\rm res},NVT;\infty}(T,P) \\ &\quad - RT\ln\left(\frac{\overline{\rho}_{\rm solv}(T,P)}{1000}\right) - RT\ln\left(\frac{RT}{100P^0}\right) \end{aligned} \tag{16}$$

Eq. (16) is the conventional means by which $\mu_{\mathrm{H^+}}^{\mathrm{res},NVT;\infty}$ is determined from experimental pK_a data for a variety of species (*e.g.*, Malloum *et al.*[26]), typically by means of continuum solvent calculations to obtain $\mu^{\mathrm{res},NVT;\infty}$ for the neutral and protonated species. (We note in passing that the term in Eq. (16) involving the solvent density is often omitted from such calculations; this is a reasonable approximation at 298.15 K for water solvent, where this term is small; however at higher temperatures and for solvents other than water, this may not be the case.) Also, since Eq. (16) requires experimental data at each temperature, such calculations have mostly been limited to 298.15 K, at which temperature data for many species is available.

In our work, we use reaction R1, whose pK_a value is identical to that of reaction R8, and for which Eqs. (8) and (9) give

$$\begin{aligned}\mu_{\mathrm{H_3O^+}}^{\mathrm{res},NVT;\infty}(T,P) &= RT\ln(10)pK_1(T,P) - \Delta G^0_{R1}(T;P^0) - \mu_{\mathrm{RNH_2}}^{\mathrm{res},NVT;\infty}(T,P) + \mu_{\mathrm{H_2O}}^{\mathrm{res},NVT;\infty}(T,P) \\ &\quad + \mu_{\mathrm{RNH_3^+}}^{\mathrm{res},NVT;\infty}(T,P) + RT\ln\left(\frac{1000}{M_{solv}}\right) \qquad (17)\end{aligned}$$

We have adjusted the $\mathrm{H_3O^+}$ FF to match the well-known experimental pK_1 value for MEA at 298.15 K and 1 bar, using FFs predicted value of hydration free energy for MEA and $\mathrm{MEAH^+}$ obtained from the GAFF/AM1–BCC and quantum chemical calculations of $\Delta G^0_{R1}(T;P^0)$. The availability of the $\mathrm{H_3O^+}$ FF then allows pK_a calculations to be performed at any temperature.

We can test the resulting $\mathrm{H_3O^+}$ FF by applying the same procedure to reaction R9, whose ΔG^* value is zero and for which Eq. (9) gives the intrinsic solvation free energy of the proton in terms of the readily calculated hydronium ion solvation value:

$$\begin{aligned}\mu_{\mathrm{H^+}}^{\mathrm{res},NVT;\infty}(T,P) &= \mu_{\mathrm{H_3O^+}}^{\mathrm{res},NVT;\infty}(T,P) - \mu_{\mathrm{H_2O}}^{\mathrm{res};\infty}(T,P) + \Delta G^0_{R9}(T,P^0) \\ &\quad - RT\ln\left(\frac{\overline{\rho}_{\mathrm{solv}}(T,P)}{1000}\right) - RT\ln\left(\frac{RT}{100P^0}\right) - RT\ln\left(\frac{1000}{M_{\mathrm{solv}}}\right) \qquad (18)\end{aligned}$$

where

$$\Delta G^0_{R9}(T, P^0) = \mu^0_{\mathrm{H_3O^+}}(T, P^0) - \mu^0_{\mathrm{H_2O}}(T, P^0) - \mu^0_{\mathrm{H^+}}(T, P^0) \tag{19}$$

This calculation is not limited to 298.15 K and 1 bar and allows $\mu^{\mathrm{res},NVT;\infty}_{\mathrm{H^+}}(T, P)$ to be readily obtained as a function of temperature and pressure.

Finally, the absolute solvation free energies of the proton and the hydronium ion may be obtained by adding the Galvani contribution, $z_i\xi_{\mathrm{G}}(T, P)$, to their respective intrinsic values, where z_i is the ion valence (+1 for $\mathrm{H^+}$), and $\xi_{\mathrm{G}}(T, P)$ is the solvent Galvani potential.

3 Computational Details

All intramolecular parameters (bond stretching, angle bending, and torsional constants) and LJ parameters(σ, ϵ) of the bicarbonate ion ($\mathrm{HCO_3^-}$), the neutral ($\mathrm{RNH_2}$), protonated ($\mathrm{RNH_3^+}$) and carbamate ($\mathrm{RNHCO_2^-}$) form of the amines were taken from the General Amber Force Field (GAFF)[27] with its default functional form using the Antechamber package in AMBER tools,[28] which assigns the parameters based on atom typing rules. Carbon dioxide ($\mathrm{CO_2}$) was modeled using the Transferable Potential for Phase Equilibrium (TraPPE) model of Potoff[29] and the solvent (water) was modeled by the TIP3P FF which is the default water model for the GAFF. We used the lowest-free-energy conformer at the G4 level as an initial structure input for calculation of partial charges. For the bicarbonate ion, we used electrostatic potential energy grid calculations at the GAFF default HF/6-31G* level using the Merz-Kollman scheme in Gaussian16 with the two-step Restrained Electrostatic Surface Potential (RESP) fitting method[30] within the Antechamber software package to assign the partial charges. For neutral ($\mathrm{RNH_2}$), protonated ($\mathrm{RNH_3^+}$) and carbamate ($\mathrm{RNHCO_2^-}$), partial charges were assigned using the Antechamber software package based on the fast semi-empirical AM1-BCC method using the G4 ideal-gas geometry. The GROMACS–formatted force field input files were then generated using the acpype (version 2019) python interface.[31] Default GAFF 1-4 interactions were used for all molecules, except for the bicarbonate ion,

for which the H–O electrostatic 1-4 interactions were scaled by 0.5 due to excessive 1-4 electrostatic interaction between these pairs.

The initial configurations for a single solute molecule solvated in a periodic box of 1500 water molecules generated using the packmol software package.[32] All MD simulations were performed using using the GROMACS (version 2016.3) program.[33] Initially, A steepest–descent minimization was performed to relax the system and remove any bad contacts, followed by a short (100 ps) NVT equilibration run followed by a 12 ns long NPT simulation with the first 2 ns discarded to determine the system density . Alchemical free energy simulations to decouple the solute molecule from its solvent environment were then started from the previously equilibrated configurations in an NVT ensemble, with simulation box size based on the calculated NPT density.

The classical equations of motion were integrated using the GROMACS stochastic Langevin algorithm, with a friction constant of 1.0 ps^{-1} and time step of 2.0 fs^{-1}. The pressure was maintained using a Parrinello-Rahman pressure coupling constant of 2.0 ps. The Lennard–Jones short–range interactions were smoothly switched off between 12 and 12.5 Å and the electrostatic interactions were computed using the particle mesh Ewald (PME) method with a 12 Å real–space cutoff, 1.0 Å grid spacing, sixth–order spline interpolation, and accuracy of 10^{-6}. The free energy of decoupling the solute molecule from its solvent environment was calculated using the GROMACS implementation of the Bennett Acceptance Ratio (BAR) method (gmx bar). We employed a linear decoupling for the electrostatic interaction with six equally spaced λ values (0, 0.2, 0.4, 0.6, 0.8, 1.0) followed by 20 equally spaced λ values (0.0, 0.05, ..., 1.0) with $\Delta\lambda = 0.05$ to decouple the LJ interactions using the standard GROMACS soft-core potential function originally proposed by Beutler et al,[34] with parameters (in GROMACS notation) *sc-alpha* = 0.5, *sc-power* = 1 and *sc-sigma* = 0.3. For each alchemical window, we used a 12.5 ns simulation with the first 2.5 ns discarded for equilibration.

3.1 Ideal–Gas Reaction Free Energies and Conformational Search

Initial conformations of the neutral, protonated and carbamate forms of the amines were generated using the Spartan v.18 software package with the default Merck Molecular Force Field (MMFF94). The 10 lowest energy conformers of each solute at the MMFF94 level were further optimized using the Gaussian 16 package, followed by frequency calculations using high–level composite methods (G4, G3, CBS-QB3 and CBS-APNO) to find the lowest-free-energy conformer for each QM method at 298.15 K. For a given QM method, the free energies of the most stable conformers were then used to calculate the ideal–gas reaction free energies at $T = 298.15$ K; to save computational time, the effect of temperature on the reaction free energy was implemented only using G4 calculations over the temperature range of 283.15–373.15 K according to:

$$\Delta G_j^0(T;P^0) = \Delta G_j^0(298.15;P^0)^{avg} + [\Delta G_j^0(T;P^0) - \Delta G_j^0(298.15;P^0)]^{\mathrm{G4}} \qquad (20)$$

where $\Delta G_j^0(298.15;P^0)^{avg}$ is the average value of the reaction free energy using G4, G3, CBS-QB3 and CBS-APNO calculations and $[\Delta G_j^0(T;P^0) - \Delta G_j^0(298.15;P^0)]^{\mathrm{G4}}$ is that of G4 calculations. We have previously shown[35] that the second term, which accounts for the effect of temperature on the ideal–gas free energy, is insensitive to the QM method/theory level; however, the absolute ideal–gas free energy of the species (the first term) can vary substantially across different QM methods. As noted previously,[25] improved predictions can arise from the use of the combination of several high–level QM methods for the calculation of this term. We therefore used the average value of $\Delta G_j^0(298.15;P^0)$ obtained from the G4, G3, CBS-QB3 and CBS-APNO calculations and the standard deviation was taken as a surrogate measure of the uncertainty of the $\Delta G_j^0(T;P^0)$ values.

4 Results and Discussion

4.1 Ideal-Gas Reaction Free Energy Changes, $\Delta G_j^0(T; P^0)$

Ideal-gas reaction free energy values $\Delta G_j^0(T, P)$ in Eq. (9) were obtained at T = 283.15, 293.15, 298.15, 303.15, 313.15, 323.15, 343.15, 353.15, 363.15 and 373.15K according to Eq. (20). We then expressed the temperature dependence of the amine deprotonation and carbamate reversion ideal-gas reaction free energies in the form

$$\frac{\Delta G_j^0(T, P^0)}{RT} = A_j^0 + \frac{B_j^0}{T} + C_j^0 \ln(T) \tag{21}$$

The coefficients of Eq. (21) for the reactions R1 and R1 are provided in Tables S1 and S2 of the Supporting Information. Fig. 3 shows the dimensionless ideal–gas reaction free energies of deprotonation (filled symbols) and for the carbamate reversion reaction (open symbols) for a primary (MEA), secondary (DEA), tertiary (TEA) and sterically hindered amine (AMP). As indicated by the R^2 values in the Supplementary Information, the data are well represented by the fitted functions. Generally, the deprotonation reaction free energy change shows more sensitivity to temperature than does that of the carbamate reversion reaction.

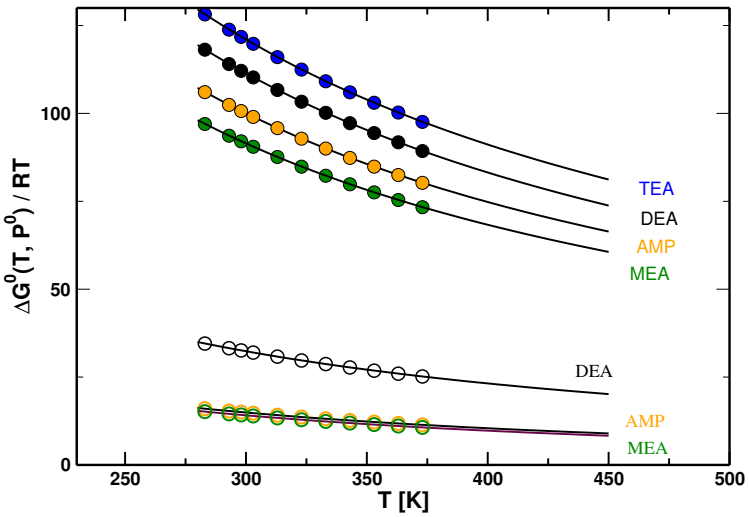

Figure 3: Ideal–gas reaction free energy change of the deprotonation reaction R1 (filled symbols) and the carbamate reversion reaction R2 (open symbols) for the indicated amines. The curves are regressions to Eq. (21).

4.2 Residual Reaction Free Energy Changes, $\Delta G_j^{\mathrm{res},NVT;\infty}(T,P)$

Calculation of the residual contribution to the reaction free energy $\Delta G_j^{\mathrm{res},NVT;\infty}(T,P)$ in Eq. (10) requires individual species $\mu_i^{\mathrm{res};\infty}(T,P)$ values as functions of temperature. While QM ideal-gas chemical potential calculations exhibit no imprecision apart from the use of different quantum theory levels, residual chemical potentials obtained from MD simulations are subject to inherent stochastic uncertainties. We have thus smoothed the individual species $\mu_i^{\mathrm{res};\infty}(T,P)$ values by regression to the functional form:

$$\frac{\mu_i^{\mathrm{res},NVT;\infty}[T,\rho(T,P)]}{RT} = a_i^{\mathrm{res}} + \frac{b_i^{\mathrm{res}}}{T} + c_i^{\mathrm{res}}\ln(T) \tag{22}$$

The coefficients $a_i^{\mathrm{res}}, b_i^{\mathrm{res}}, c_i^{\mathrm{res}}$ for all species, including the small molecules (H_2O, CO_2, HCO_3^-, H_3O^+), are provided in Tables S3–S6 of the Supplementary Information. The coefficients $A_j^{\mathrm{res}}, B_j^{\mathrm{res}}, C_j^{\mathrm{res}}$ in Eq. (14) for reaction j are then obtained from

$$A_j^{\mathrm{res}} = \sum_{i=1}^{N_s} \nu_{i,j} a_i^{\mathrm{res}} \tag{23}$$

$$B_j^{\text{res}} = \sum_{i=1}^{N_s} \nu_{i,j} b_i^{\text{res}} \tag{24}$$

$$C_j^{\text{res}} = \sum_{i=1}^{N_s} \nu_{i,j} c_i^{\text{res}} \tag{25}$$

For the majority of solutes considered in this work, the μ_i^{res} regressions are of good quality, as indicated by their R^2 values. However, larger flexible molecules with multiple conformers in the solution exhibit somewhat scattered μ_i^{res}/RT values. For these molecules, we performed five independent replicate simulations (each using different random–number seeds to generate the initial configuration and the initial atomic velocity assignment), and we used the resulting average μ_i^{res}/RT values in the regression. We show a typical result for such a larger molecule in Fig. 4.

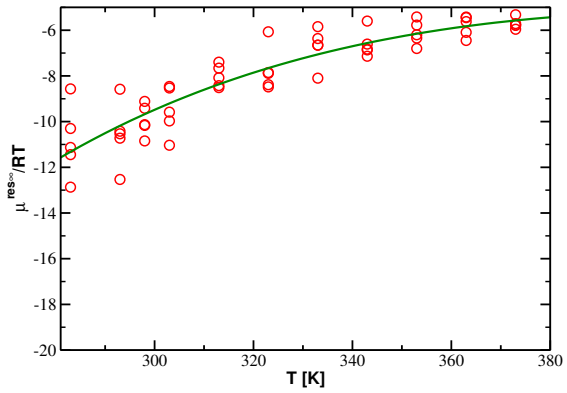

Figure 4: Infinite dilution residual chemical potential of the neutral 4IPB as a function of temperature from five replicate simulations at each temperature. The curve is the result of fitting Eq. (22) to the simulation data using the average value at each temperature.

4.3 Deprotonation Constant, pK_a

A parity plot of predicted versus experimental pK_a data is shown in Fig. 5. The dashed line indicates a tolerance of 1.0 pK_a unit, and for most of the considered amines the error is less than 1.0 pK_a unit, equivalent to an error of $\approx$ 5.7 kJ·mol^{-1} in the reaction free energy at

T=298.15 K.

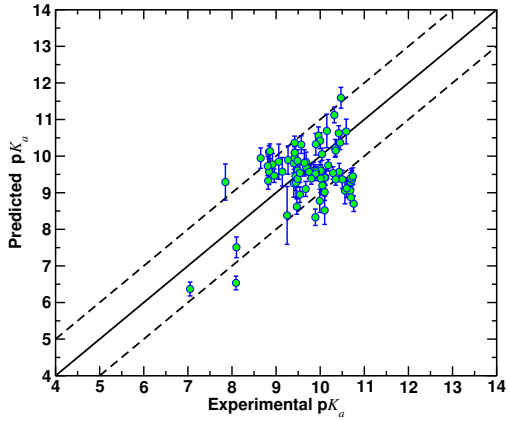

Figure 5: Calculated versus experimental pK_a values for the 77 alkanolamine species considered in this work. The vertical error bars are obtained by propagating the uncertainty in the ideal–gas reaction free energy (horizontal error bars for the experimental data are not shown) and the dashed line indicates a tolerance of 1.0 pK_a unit.

Table 1 summarizes the numerical values of the protonation constant of the 77 studied amine at 298.15 K, along with the carbamate formation constant of the primary and secondary amines obtained in this work. The experimental pK_a data were taken from the literature.[6–8,36–43] Using the developed H_3O^+ FF, we found an average absolute deviation (AAD) of 0.72 pK_a units for a set of 77 amines. Our results show that the pK_a values of amines with multiple hydroxyl groups are underestimated and those of alkyamines (amines with no hydroxyl group) are overestimated.

Table 1: Protonation and carbamate formation constants of the studied amines at T = 298.15 K. The uncertainty in the simulation values is based on the uncertainty in the ideal gas contribution to the reaction free energy, since that of the residual part is negligible. The uncertainty in the experimental pK_a data is typically smaller than 0.1 pK unit and that for the carbamate formation is inferred to be around the MEA value of $\approx$ 0.25 pK_a unit. t indicates tertiary amines, which do not form carbamate.

	pK_a		pK_c	
Amine	this work	literature	this work	literature
1AB	$9.26_{0.38}$	9.4	$1.62_{0.27}$	
1AP	$9.27_{0.40}$	9.45	$1.53_{0.28}$	1.70[44]
2AB	$9.89_{0.39}$	9.27	$1.32_{0.30}$	
2AEE	$10.36_{0.18}$	9.42	$3.78_{0.34}$	

Continued on next page

Table 1 – *Continued from previous page*

	pK_a		pK_c	
Amine	this work	literature	this work	literature
2AP	$9.81_{0.26}$	9.4	$0.75_{0.15}$	0.60,[44] 0.98[4]
2DIPA	$9.95_{0.20}$	9.42	t	
2MPA	$9.36_{0.25}$	10.5	$1.28_{0.11}$	
2PIPE	$10.63_{0.20}$	10.42	$-0.19_{0.40}$	no carbamate detected[4]
2PIPM	$9.42_{0.22}$	10.12	$-0.06_{0.32}$	no carbamate detected[4]
3AP	$10.56_{0.24}$	9.96	$2.07_{0.15}$	1.83[44]
3DMAP	$9.61_{0.26}$	9.49	t	
3PIPM	$9.20_{0.26}$	10.05	$4.23_{0.33}$	
4AB	$11.12_{0.21}$	10.32	$1.87_{0.35}$	
4PIPM	$9.06_{0.36}$	10.56	$1.88_{0.33}$	1.39[4]
AEPD	$9.33_{0.23}$	8.82	$-0.39_{0.38}$	
AMPD	$9.57_{0.35}$	8.84	$0.98_{0.32}$	no carbamate detected[4]
AMP	$9.84_{0.27}$	9.68	$0.16_{0.21}$	no carbamate detected[4]
DA	$8.70_{0.21}$	10.76	$1.10_{0.75}$	
DEA	$9.77_{0.30}$	8.92	$1.57_{0.46}$	0.92[4]
DIPA	$10.11_{0.17}$	8.84	$1.91_{0.40}$	
DMIPA	$8.62_{0.21}$	9.47	t	
EAE	$9.65_{0.19}$	10	$1.53_{0.32}$	
EAMP	$10.42_{0.22}$	10	$-1.57_{0.57}$	
EDA	$10.33_{0.30}$	9.9	$0.42_{0.29}$	
IBAE	$9.60_{0.16}$	10.01	$2.93_{0.24}$	
IPAE	$9.61_{0.15}$	9.78	$0.16_{0.28}$	
IPA	$9.06_{0.23}$	10.68	$-0.30_{0.10}$	
MAE	$9.60_{0.23}$	9.85	$2.42_{0.60}$	
MDEA	$9.95_{0.28}$	8.65	t	
MEA	$9.46_{0.39}$	9.44	$1.61_{0.25}$	1.6, 1.81, 1.76, 1.31, 1.25[4,5,9,45,46]
MPAE	$10.10_{0.16}$	9.42	$1.13_{0.36}$	
nCHEA	$9.41_{0.16}$	10.1	$-0.21_{0.26}$	
nCPEA	$6.53_{0.19}$	8.09	$-0.30_{0.54}$	
nCPnEA	$9.02_{0.23}$	10.1	$-1.01_{0.28}$	
PA	$9.12_{0.25}$	10.6	$0.81_{0.10}$	2.20[44]
SAPD	$9.73_{0.24}$	8.55	$1.05_{0.25}$	no carbamate detected[4]
TBAE	$10.05_{0.16}$	10.04	$-2.61_{0.63}$	
TBA	$9.57_{0.23}$	10.43	$-0.77_{0.66}$	
tBDEA	$9.85_{0.48}$	9.06	t	
TREA	$8.87_{0.14}$	10.7	t	
12HEPP	$10.31_{0.24}$	9.57	t	
1DEA2P	$9.75_{0.15}$	10.18	t	
1DMA2P	$9.10_{0.20}$	9.67	t	
1M2PPE	$8.33_{0.22}$	9.89	t	
1PE	$9.46_{0.18}$	8.96	t	

Continued on next page

Table 1 – *Continued from previous page*

	pK_a		pK_c	
Amine	this work	literature	this work	literature
1PP	$9.38_{0.23}$	9.49	t	
3DEA1P	$9.54_{0.17}$	10.29	t	
3MDA1P	$9.54_{.25}$	9.54	t	
3PPE	$9.87_{0.30}$	9.49	t	
4IPB	$10.37_{0.19}$	10.45	$-0.34_{0.38}$	
5AP	$11.59_{0.28}$	10.47	$3.17_{0.40}$	
6AH	$10.67_{0.33}$	10.59	$5.35_{0.36}$	
BAE	$9.58_{0.18}$	9.9	$1.54_{0.32}$	
BA	$9.29_{0.25}$	10.69	$0.85_{0.11}$	1.7[44]
DEA12PD	$9.70_{0.20}$	9.68	t	
DEAB	$9.36_{0.15}$	10.35	t	
DEAEEO	$10.69_{0.46}$	10.15	t	
DMA12PD	$9.57_{0.38}$	9.14	t	
DMA22DP	$8.95_{0.21}$	9.54	t	
DMA2M1P	$10.21_{0.24}$	10.34	t	
DMAH	$9.39_{0.38}$	10.01	t	
EDEA	$10.13_{0.20}$	8.86	t	
DEEA	$9.57_{0.17}$	9.75	t	
IBA	$9.35_{0.25}$	10.72	$1.34_{0.11}$	1.98[44]
IPAP	$10.15_{0.15}$	10.35	$0.48_{0.31}$	
PA2	$9.40_{0.25}$	10.7	$1.01_{0.11}$	
PAE	$9.52_{0.18}$	9.89	$2.73_{0.31}$	
PRLD12PD	$9.82_{0.36}$	9.64	t	
PRYE	$9.39_{0.15}$	9.8	t	
SBA	$9.45_{0.23}$	10.74	$0.13_{0.08}$	1.32[44]
TEA	$9.29_{0.50}$	7.85	t	
TMPOL	$8.78_{0.31}$	9.99	$-6.48_{0.70}$	
TRC	$7.51_{0.28}$	8.1	$-0.90_{0.80}$	
3QCD	$8.52_{0.38}$	10.1	t	
AMN	$8.38_{0.79}$	9.25	$1.2_{1.03}$	
2MORE	$6.37_{0.20}$	7.05	t	

4.4 Temperature Dependence of pK_a and the Deprotonation Standard Reaction Enthalpy

Figs. 6 and Fig.7 show the temperature dependence of the MEA pK_a and of the amines for which we found experimental temperature dependent pK_a data, namely AMP, 1-AP, DEEA, MAE, 2DIPA, 2AP, 3DMA1P employing our H_3O^+ FF. The data shows that the developed H_3O^+ FF is able to accurately predict the temperature trend despite the fact that only the pK_a of MEA at $T = 298.15$ K was used to train it.

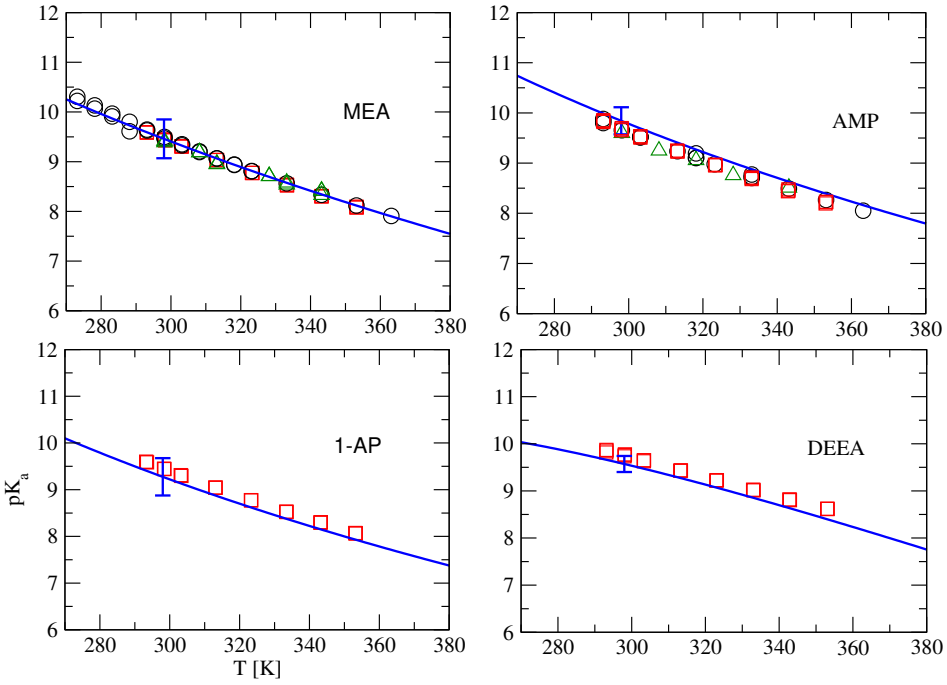

Figure 6: Deprotonation constants of monoethanolamine(MEA), 2-amino-2-methyl-1-propanol (AMP), 1-amino-2-propanol (1-AP) and diethylethanolamine (DEEA) as functions of temperature. Experimental data is shown by a circle,[38] square[6] and triangle up,[41] and the curves are our simulation results. The error bars indicate the uncertainty at 298.15 K indicated in the caption to Table 1.

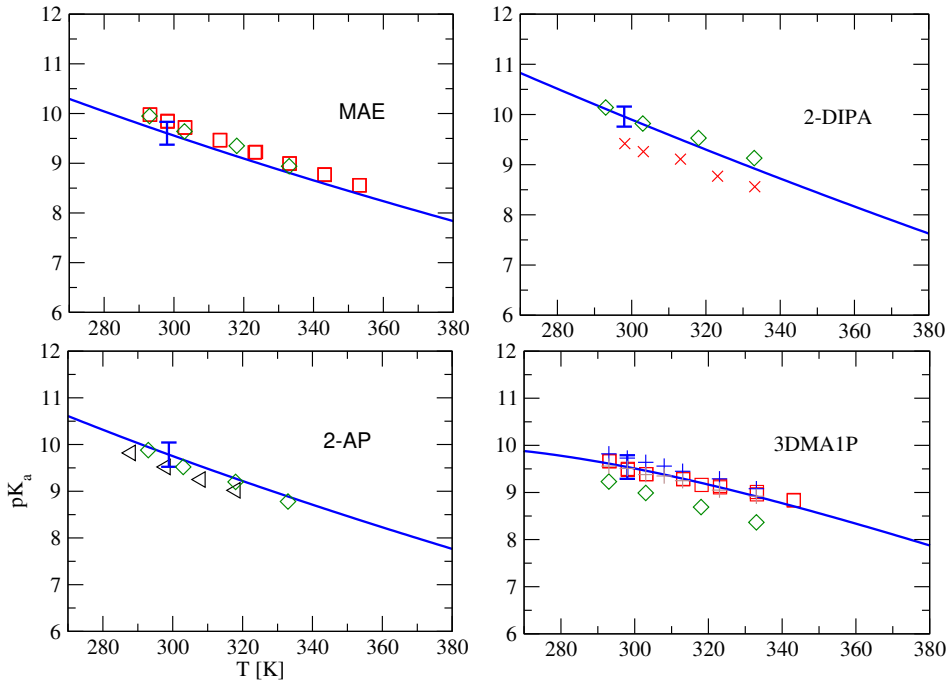

Figure 7: Deprotonation constants of methylaminoethanol(MAE), 2-(diisopropylamino)ethanol (2-DIPA), 2-amino-1-propanol (2-AP) and 3-dimethylamino-1-propanol (3DMA1P) as functions of temperature. Experiemental data are shown by a square,[6] diamon,[39] triangle left[8] plus[36] and star,[37] and the curves are our simulation results. The error bar indicates the uncertainty at 298.15 K indicated in the caption to Table 1.

As shown in Figs. 8–9, for the molecules with multiple hydroxyl groups, namely TBAE, 2AEE, EAE, AEPD, AMPD, DEA, SAPD, the pK_a simulations overestimate the experimental results. Since the ideal gas and the residual chemical potentials both contribute to the resulting pK_a values, we are not able to pinpoint the source of the error, and it could be due to the well-known issue with the amine hydroxyl parameters of the GAFF and its hydration free energy prediction,[47] or due to the error in the ideal gas QM prediction for species with multiple oxygen atoms, which are subjected to relatively larger uncertainty, as in the case of TEA with three hydroxyl groups.

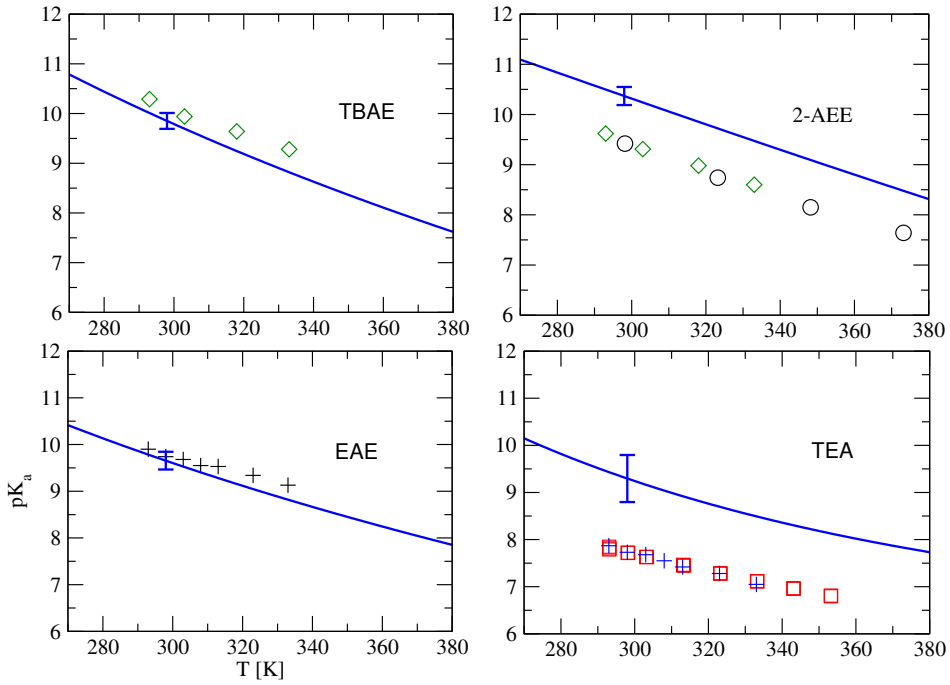

Figure 8: Deprotonation constant of 2-(tert-butylamino)ethanol (TBAE), 2-(2-aminoethoxy)ethanol (2-AEE),2-(ethylamino)ethanol (EAE) and triethanolamine (TEA) as function of temperature. Experimental data is shown by square,[6] diamon,[39] triangle left[8] plus[36] and star,[37] and the curves are our simulation results. The error bar indicates the uncertainty at 298.15 K from the caption to Table 1.

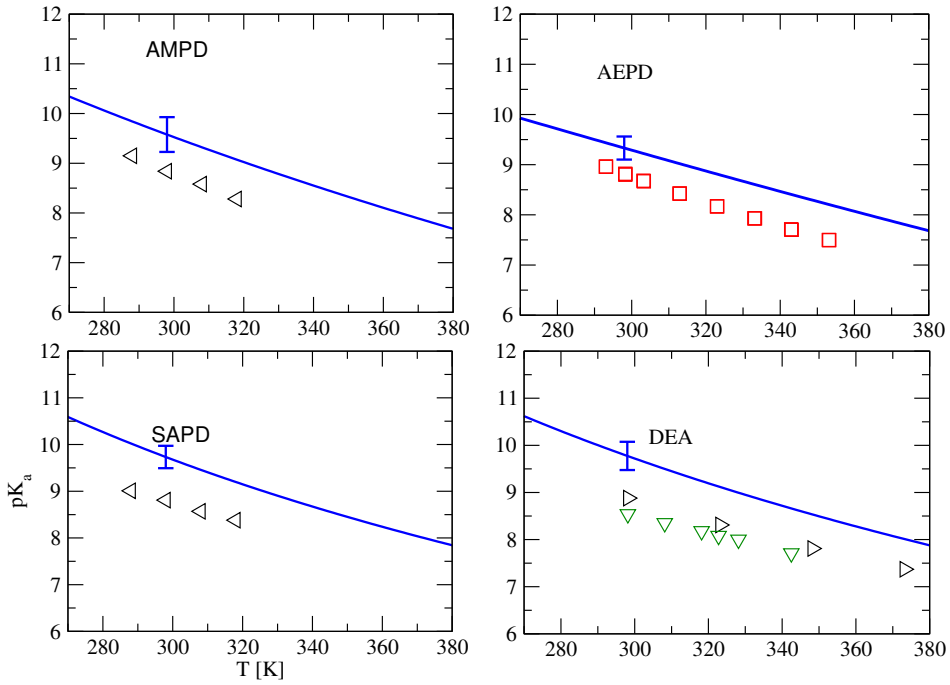

Figure 9: Deprotonation constant of 2-amino-2-ethyl-1,3-propanediol (AEPD), 2-amino-2-methyl-1,3-propanediol (AMPD),diethanolamine (DEA) and serinol(2-aminopropane-1,3-diol) (SAPD) as function of temperature. Experimental data is shown by square,[6] diamond,[39] triangle left[8] plus[36] and star,[37] and the curves are our simulation results. The error bar indicates the simulation uncertainty at 298.15 K from the caption to Table 1.

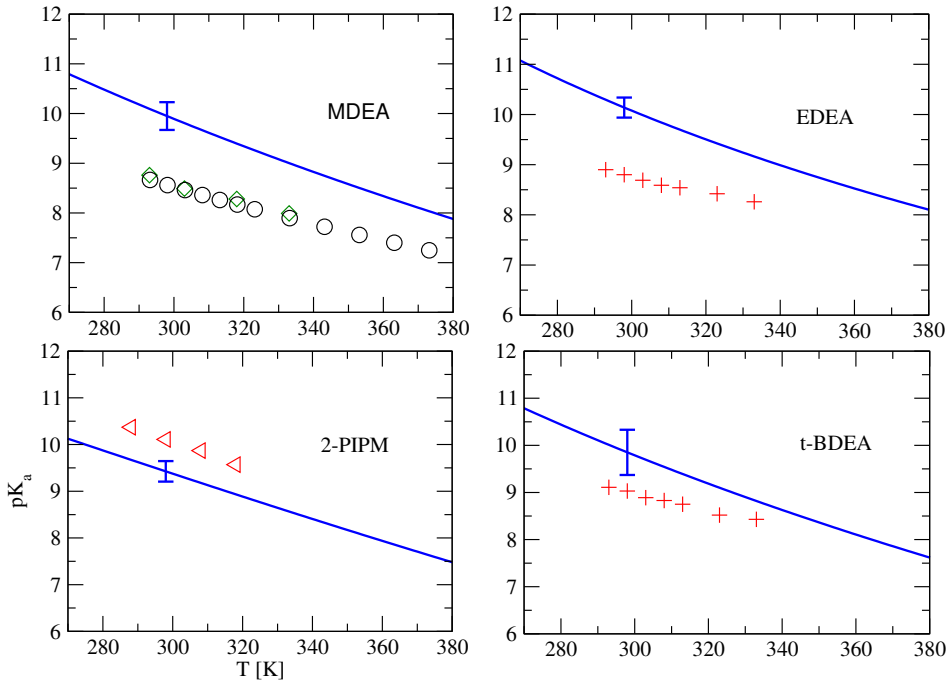

Figure 10: Deprotonation constant of methyldiethanolamine (MDEA), n-ethyldiethanolamine (EDEA),2-piperidinemethanol (2PIPM) and tert-butyldiethanolamine (t-BDEA) as function of temperature. Experimental data is shown by square,[6] diamond,[39] triangle left[8] plus[36] and star,[37] and the curves are our simulation results. The error bar indicates the uncertainty at 298.15 K from the caption to Table 1.

The Gibbs–Helmholtz (G–H) equation relates the equilibrium constant of the reaction to its standard reaction enthalpy, via.

$$-\Delta H_j^{\dagger}(T,P) \;=\; -RT^2\left(\frac{\partial \ln K_j}{\partial T}\right) = R[-(B_j^0+B^{\rm res})+(C_j^0+C_j^{\rm res})T] \qquad (26)$$

The coefficients of $-\ln K_j$ and $-\Delta H_j^{\dagger}(T,P)$ of the deprotonation reaction obtained from the coefficients of the ideal gas free energy function (A_j^0, B_j^0, C_j^0) and the residual free energy function (A^{res}, B^{res}, C^{res}) of the corresponding reaction according to Eq. (14) and Eq. (26) are given in Tables S7. The reaction enthalpy data at a typical absorption temperature ($T = 313.15$ K) is given in Table S9.

We remark that most literature studies have measured the equilibrium constant over a narrow temperature range around $T = 298.15$ K and assumed a constant reaction enthalpy, obtained from vant Hoff–type equation of $\ln K$ against 1/T data.[48] This is only valid over the small temperature range at which experimental $\ln K$ measured and should be compared to our values at $T = 298.15$ K.

We previously have shown that the uncertainty in the IG reaction enthalpies is very similar to that of the IG reaction free energies,[35] for which we used the standard deviation of the IG results from G4, G3, CBS-QB2 and CBS-APNO calculations as a surrogate uncertainty measure. The data in Table 1 indicate that the IG contribution to the uncertainty in the deprotonation reaction enthalpies at 298.15 K is smaller than 0.5 pK_a unit (≈ 2.85 kJ) in all cases. Table 2 compares the simulation values of the de-protonation reaction enthalpy of the amines for which there is experimental data. Due to the sensitivity of the reaction enthalpy to the $\ln K$ data (which is subject to experimental uncertainty) there is significant scatter in the experimental reaction enthalpy data, however, our simulation values are in reasonable agreement with the available experimental data.

Table 2: Enthalpy of deprotonation of amines (ΔH^{deprot}/kJ.mol^{-1}) in aqueous solution at 298.15 and 313.15 K. The uncertainty in the simulation values are smaller than $\approx$ 2.85 kJ in all cases.

Amine	T=298.15 K		T=313.15 K
	This work	Literature	This work
MEA	45.64	48.6[6] 43.0[7] 41.0[8] 50.5[49] 50.89[41]	47.60
AMP	50.70	52.2[6] 46.6[8] 40.61[7] 53.99[50]	52.07
AMPD	44.33	47.2[8] 49.85[51]	46.65
AEPD	35.81	47.5[6]	38.90
3-AP	52.92	53.6[6]	53.57
MAE	40.50	44.4[6]	42.97
1-AP	46.72	48.8[6]	48.11
2-AEE	43.95	50.2[6]	48.09
DEA	47.46	42.4[6] 37.5[8] 38.71[7] 42.4[52]	48.54
DIPA	50.40	39.2[6]	52.48
2-DIPA	51.73	46.50[37]	55.67
2-AP	45.49	47.0[8]	48.90
3DMA1P	25.78	28.07[7] 30.81[36]	33.06
EAE	43.50	33.86[36]	45.15
SAPD	47.94	37.8	48.74
DEEA	31.76	36.2[6] 34.22[36]	38.25
DMIPA	34.84	36.99[36]	36.56
TEA	45.40	31.3[6] 32.0[8] 34.0[53] 31.59[7]	-43.77
MDEA	48.70	34.9[6] 36.0[8] 33.37[7]	51.11
EDEA	52.17	28.97[36]	52.83
TREA	54.14	45.60[36] 44.4[6]	49.16
t-BDEA	53.60	33.02[36]	55.77
2-PIPM	42.12	46.0[8]	45.84
3-PIPM	41.60	40.3[8]	41.91
4-PIPM	28.22	34.0[8]	33.78
2-PIPE	36.81	37.0[8]53.8[54]	48.08

4.5 Carbamate reversion constant, (pK_c)

Carbamate reversion into bicarbonate is one of the major chemical reactions involving CO_2 absorption occurring in primary and secondary amine based solutions. The results for the carbamate reversion reaction pK R2 (the negative of the carbamate formation reaction value) for the primary and secondary amines are summarized in Table 1, and compared with

scarcely available experimental determinations at 298.15 K. We remark that the equilibrium constant is composition-independent quantity which may be directly predicted from simulation quantities at infinite dilution. On the other hand, this quantity cannot be directly measured experimentally, but must be obtained indirectly from concentration measurements at finite compositions $\mathbf{m}^*$, governed by

$$\ln K_j(T,P) \quad = \quad \sum_{i=1}^{N_s}[\nu_{ij}[\ln m_i^* + \ln \gamma_i(T,P;\mathbf{m}^*)] \tag{27}$$

which requires the use of an activity coefficient model. Unlike the case for the deprotonation reaction, it is problematic to extrapolate results obtained for the carbamate reaction using Eq. (27) to infinite dilution, since in CO_2-loaded aqueous amine solutions, the carbamate reversion reaction cannot be isolated and the bicarbonate and carbamate ions co-exist with other ions (i.e, OH^- , H_3O^+, CO_3^{-2} etc). At relatively low CO_2 loadings (low ionic strength), the activity coefficients of the bicarbonate and carbamate ions approach unity and at low amine weight fractions, only the activity coefficient data of binary amine/water system (at relatively low amine weight fraction, where only amine infinite dilution activity coefficients are required) along with the equilibrium composition maybe used in the Eq. (27) to estimate the equilibrium constant. An approximation often made for isocoulombic reactions (with ions on each side of the reaction having the same charge, which is the case for the carbamate reversion reaction) is to assume that the activity of water is unity and the activity coefficients of $RNHCO_2^-$ and HCO_3^- are equal (as is the case for the Debye-Hückel; and other simple activity coefficient models). In this case, the activity coefficient terms in Eq. (27) cancel at all concentrations.

Another approach is to fit the experimental VLE data (CO_2 partial pressure and speciation data) to the parameters of a thermodynamic model for the chemical potentials to obtain the equilibrium constant. As a result of the different approximation approaches, the spread of the literature values is partly due to differences in the activity coefficient models

used by the authors, and more likely due to the difficulty in the experimental NMR measurement of the concentrations of the bicarbonate ion and neutral amine species, which is difficult to distinguish from the protonated and carbonate ion in the NMR peaks. The experimental carbamate formation constant data are limited and likely subject to significant uncertainty. For example, carbamate formation constants of MEA have been measured using various experimental methodology including NaOH titration of the carbamate solution,[5] fitting thermodynamic models to vapour-liquid-equilibrium (VLE) data of CO_2-loaded solutions, and to CO_2 partial pressure data,[45,55,56] NMR titrations,[10] calorimetric studies and H-NMR Spectroscopy,[4] giving values ranging from 1.31[5]-1.85.[4] We compare our predicted values with the scarcely available experimental data in Table 1. Given the lack of the pK_c data from different measurement, based on the MEA data, we infer the uncertainty in the experimental to be $\approx$ 0.25 pK unit comparable to that of the simulation data. Lack of comprehensive and accurate experimental pK_c data complicates fair comparison with the simulations data. Overall, our predictions are in reasonable agreement with the available experimental data.

4.6 Effect of Structural Features on Carbamate Reversion

The effect of structural feature modifications with respect to those of MEA on the extent of carbamate formation may be explained, allowing us to identify structural factors of alkanolamine molecules that influence the CO_2 absorption properties. The increasing trend in the carbamate reversion constants of MEA (pK_c= 1.61± 0.25), 3-AP (pK_c= 2.07± 0.15), 4-AB (pK_c= 1.87± 0.35), 5AP (pK_c= 3.17±0.40) and 6-AH (pK_c= 5.35±0.36) indicates that increasing the chain length promotes carbamate formation. The addition of a -CH_3 and -C_2H_5 group on the β carbon of MEA gives 1-AP (pK_c= 1.53 ±0.28) and 1AB (pK_c= 1.62 ±0.27) respectively, with a carbamate reversion constant similar to that of MEA, indicating that the steric effect of the β carbon is not significant. However, addition of the same -CH_3, -C_2H_5 and -CH_2(OH) groups on the β carbon of MEA gives 2-AP (pK_c= 0.75 ±0.15) and

2-AB (pK_c= 1.32 ±0.30) and SAPD (pK_c= 1.05 ±0.25), respectively, significantly lowering their tendency to form carbamate. AMP (pK_c= 0.16 ±0.21), AMPD (pK_c= 0.98 ±0.32) and AEPD (pK_c= -0.39 ±0.38) are heavily hindered derivatives of MEA, and all show little or no tendency to form carbamate as predicted by the molecular models.

The addition of various alky chain groups on the nitrogen atom of MEA gives the primary amines MAE (pK_c=2.42 ±0.60), EAE (pK_c= 1.53 ±0.32), BAE (pK_c= 1.54 ±0.32), IPAE (pK_c= 0.16 ±0.28) and TBAE (pK_c= -2.61 ±0.63), clearly indicating that the longer and more branched the alkane chain, the more unstable is the amine carbamate (pK_c becomes more negative). Compared to EAE, EAMP (pK_c= -1.57±0.57) has two additional CH_3 groups in the α carbon, significantly lowering its pK_c.

n-CHEA (pK_c= -0.21±0.26), nCPEA (pK_c= -0.30±0.54) and nCPnEA (pK_c= -1.01±0.28) are obtained by a adding a six-, five- and three-membered ring structure to the amine group of MEA. They all show a negative carbamate reversion constant, indicating that the addition of the ring group makes the carbamate formation extremely unstable.

In the case of the primary alkyamines, PA (pK_c= 0.81 ± 0.10), BA (pK_c= 0.85 ±0.11), PA2 (pK_c= 1.01 ±0.11), IBA (pK_c= 1.34 ± 0.11), SBA (pK_c= 0.13 ±0.08), IPA (pK_c= -0.30± 0.10) and TBA (pK_c= -0.77 ± 0.66), the effect of the steric hindrance of the methyl group is in line with the decreasing pK_c.

For the cyclic amine 2PIPM (pK_c= -0.06± 0.32), 2PIPE (pK_c= -0.19± 0.40), due to proximity of the amino and hydroxyl group, it chemically easier to form intra-molecular hydrogen bonds, and this has been shown to reduce the stability of carbamate formation [57] by formation of stable ring structure that maximize internal hydrogen bonding , consistent with their predicted negative pK_c values. This is also in agreement with the H-NMR spectroscopy measurements of Fernandes*et al.*, who did not detect carbamate formation in aqueous 2PIPM and 2PIPE. However, in case of 4PIPM (pK_c= 1.88 ± 0.33), the amino group is located far from the hydroxyl and results in a higher pK_c, in excellent agreement with the Fernandes*et al.*measured value of 1.39. Overally, we believe the molecular models employed in this work

is able to predict the trend in the carbamate formation tendency of amines.

4.7 Temperature Dependence of pK_c and the Carbamate Reversion Standard Reaction Enthalpy (ΔH^{carb})

Given the complications associated with the accurate experimental measurement of the carbamate reversion (inverse of carbamate formation reaction) constant, the experimental carbamate reversion enthalpy (ΔH^{carb}), which obtained from the temperature derivative of its equilibrium constant, expected to have much larger errors associated with them. For example, the literature value of MEA experimental ΔH^{carb}/kJ·mol^{-1} obtained from Van't Hoff analysis of the equilibrium constant data over a narrow temperature range ranges from 12.84[5]kJ·mol^{-1} to 29.7[9] kJ·mol^{-1}. Similarly for DEA, different analysis methods for the experimental measurements[4,9,45] give values ranging from 13.64[45] kJ·mol^{-1} to 23.7[9] kJ·mol^{-1}. Fig.11 shows the temperature dependence of the MEA pK_c from our simulations (red curve) and its comparison with the most recent studies of Fernandes[4](circles) and Böttinger[45](blue curve). Our predictions agree well with the experimental data from other sources[9,56,58] shown by different symbols. While the most literature studies assume constant (ΔH^{carb}), our simulation indicate slight temperature dependency for ΔH^{carb} (change of $\approx$ 2.0 kJ over T change of $\approx$ 100 K).

The ideal gas contribution to the uncertainty of ΔH^{carb} is much larger than the deprotonation reaction(ΔH^{deprot}) as indicated in Table 1 ranging from 0.1-1.0 pK unit or $\approx$ 0.57-5.7 kJ at T=298.15 K. The coefficients of $-\ln K_c$ and ΔH^{carb} obtained from the coefficients of the ideal gas free energy function (A_j^0, B_j^0, C_j^0) and the residual free energy function (A^{res}, B^{res}, C^{res}) of the reversion reaction according to Eq. (14) and Eq. (26) are given in Tables S8 of Supplementary Information. The reaction enthalpy data at a typical absorption temperature ($T = 313.15$ K) is given in Table S9. The ΔH^{carb} and ΔH^{deprot} data maybe used in conjunction with the readily available enthalpy data of reactions R3-R6 to estimate overall heat of CO_2 absorption in these amines.

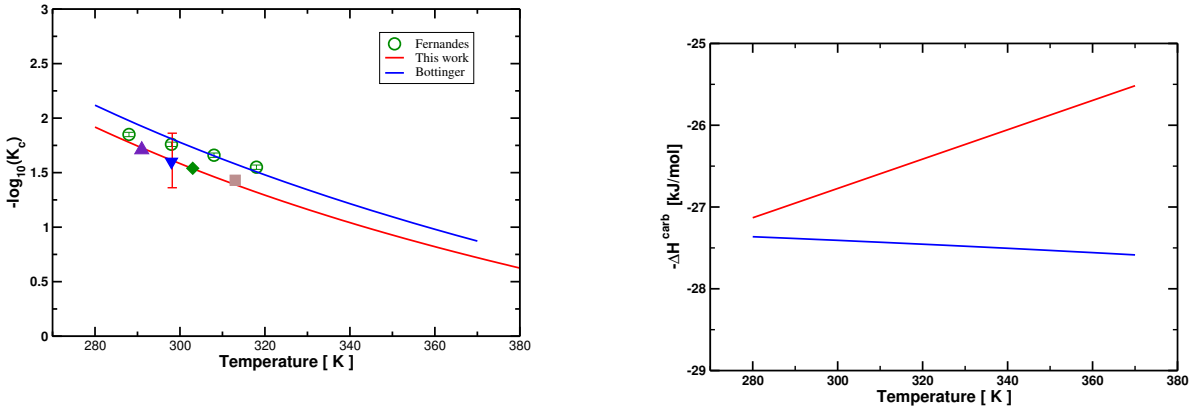

(a) (b)

Figure 11: (a) Comparison of the equilibrium constant of the MEA carbamate reversion reaction (R2) of this work (red curve) with the experimental data of Bottinger[45] (blue curve), fernandes[4] (open green circles) and other symbols are from[9,56,58]
. (b) the corresponding reaction enthalpies of carbamate reversion reaction R2.

Table 3: Enthalpy of carbamate reversion (ΔH^{carb}/kJ·mol^{-1}) of amines in aqueous solution at 298.15 (subscripts indicates the uncertainty of ideal gas contribution to reaction enthalpy) and 313.15 K.

Amine	T=298.15 K		T=313.15 K
	This work	Literature	This work
MEA	$26.80_{1.40}$	29.7[9] 18.0[4] 27.40[45] 12.84[5]	26.53
2-AP	$16.86_{0.85}$	27[4]	17.60
DEA	$14.28_{2.62}$	18.0[4] 13.64[45] 23.7[9]	15.51

4.8 Validation of the H_3O^+ Force Field Using its Prediction of the Proton Hydration Free Energy

Most pK_a studies in the literature are restricted to T = 298.15 K, where a theoretically obtained literature value for the proton hydration free energy (*e.g.*, that of Tissandier *et al.*[24]) is typically used to predict the pK_a. However, a classical FF for the H_3O^+ ion allows the prediction of this quantity over a temperature range, including the elevated temperatures of interest to carbon capture processes. Other studies have calculated pK_a at T = 298.15 K with respect to a reference acid and then used the experimental temperature dependence

of the reference acid to accomplish this task. However, the reference acid experimental data at high temperatures might not be readily available or one might want to look at different solvents, requiring reference acid temperature–dependent pK_a data for each solvent.

In our study, we have developed an H_3O^+ force field to reproduce the well-known experimental pK_a value of 9.44 ± 0.05 for MEA (in water solvent) at 298.15 K. This allows the calculation of the temperature dependence of its hydration free energy. We first calculated its theoretical ideal–gas deprotonation reaction free energy value of 228.21±2.24 kJ·mol^{-1} (taken as the average of CBS-QB3, G4, G3 and CBS-APNO calculations), the MEA and MEAH$^+$ AM1–BCC hydration free energy values (-28.56 ± 0.10 and -246.25 ± -0.250 kJ·mol^{-1}, respectively), and the TIP3P H_2O self–solvation free energy (-26.82 ± 0.08 kJ·mol^{-1}). From this data, Eqs. (8)-(12) yield an H_3O^+ intrinsic hydration free energy of -408.84± 2.3 kJ·mol^{-1}. Finally, using the TIP3P LJ parameters of water and the non-bonded parameters of Váchа*et al.*[59] for the H_3O^+ FF, we adjusted its oxygen partial charge to reproduce this value. The details of the resulting H_3O^+ FF are given in the Supplementary Information.

We validated our H_3O^+ FF by comparing several of its intrinsic hydration free energy with the literature results. Using the values from CBS-APNO, CBS-QB3, G3 and G4 calculations of the water basicity $-\Delta G^0_{R9}(T, P^0)$ in Eq. (18) (662.83, 657.76, 661.40 and 662.98 kJ·mol^{-1}), we obtained an average value of $\Delta G^0_{R9}(T, P^0) = -661.24 \pm 2.43$ kJ·mol^{-1}. This agrees well with the Hunter and Lias[60] value of -660 kJ·mol^{-1} recommended by the NIST Chemistry Webbook,[61] *ab initio* values of -662.74 kJ·mol^{-1} obtained by Palascak and Shields[62] and a best estimate of -658.14 kJ·mol^{-1} by Zhan and Dixon.[63]

Using the TIP3P water simulation properties of density (ρ = 987.562 kg·m^{-3}), its self-solvation free energy ($\mu^{\mathrm{res},NVT;\infty}_{H_2O}$ =-26.82± 0.08 (which is close to the experimental value of -26.44 kJ·mol^{-1} given by Camaioni[64]), and the Galvani potential value of ξ_G = -48.24 kJ·mol^{-1},[65,66] Eq. (18) gives the value $\mu^{\mathrm{res},NVT;\infty}_{H^+}(298.15\ \mathrm{K}, 1.0\ \mathrm{bar}) = -1109.38 \pm 2.43$ kJ·mol^{-1} for the proton absolute hydration free energy. This agrees well with the most well–established experimental value of -1112.5 kJ·mol^{-1} of Tissandier*et al.*[24]

Assuming that the Galvani potential is invariant with respect to temperature, Fig. 12 shows the intrinsic and absolute values of the proton solvation free energies and enthalpies as functions of temperature.

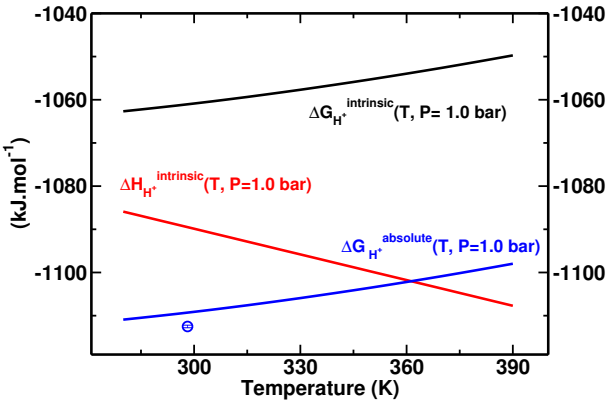

Figure 12: Intrinsic hydration free energy (black curve), intrinsic hydration enthalpy (red curve) and absolute hydration free energy of the proton (blue curve) as functions of temperature, assuming that that the water Galvani potential of the water is invariant with temperature. The filled blue circle indicates the value of Tissandier *et al.*[24]

Table 4: Coefficients of the function $A + B/T + C\ln(T)$ fitted to $\Delta G^0_{R9}(T, P^0)/RT$, $\ln\left(\frac{\overline{\rho}_{\rm solv}(T,P)RT}{100P^0 M_{solv}}\right)$, $\mu^{res,\infty}_{H_2O}/RT$, $\mu^{res,\infty}_{HCO_3^-}/RT$, $\mu^{res,\infty}_{H_3O^+}/RT$ $\mu^{res,\infty}_{H^+}/RT$ terms in Eq.18 .

molecule/ion	**A**	**B**	**C**	R^2
$\Delta G^0_{R9}(T, P^0)/RT$	-235.09	-70902.4	36.1984	0.001
$\ln\left(\frac{\overline{\rho}_{\rm solv}(T,P)RT}{100P^0 M_{solv}}\right)$	9.85008	-305.675	-0.282471	0.008
$\mu^{res,\infty}_{H_2O}/RT$	27.2591	-5988.09	-3.15944	0.0013
$\mu^{res,\infty}_{HCO_3^-}/RT$	-99.6984	-48119.3	17.9077	0.0337
$\mu^{res,\infty}_{H_3O^+}/RT$	124.002	-59320.3	-15.7999	0.0330
$\mu^{res,\infty}_{H^+}/RT$	-148.19718	-123928.935	23.840411	-

5 Conclusions and Recommendations for Future Work

We have refined our previously developed[21] general framework for prediction of the equilibrium constants of chemical reactions in solution applied to CO_2–loaded aqueous amine solutions. The primary aspect of the refinement is the use of *isocoulombic* reactions to predict the deprotonation and carbamate reversion equilibrium constants and their temperature dependence; this use of such reactions is in concordance with the recent finding that such reactions enable improved estimates of the temperature trend of equilibrium constants.[22]

This approach requires the development of a new H_3O^+ (hydronium) force field (FF) for the deprotonation reaction. We developed this FF by matching the well-known monethanolamine deprotonation equilibrium constant value at 298.15 K, which involved adjusting the GAFF oxygen atom partial charge. We are thereby able to predict the pK_a of a diverse set of 77 amines at 298.15 K and all other temperatures by the appropriate combination of ideal-gas and residual chemical potential values for the deprotonation reactions. The predictions at 298.15 K show an absolute average deviation (AAD) with respect to experimental values of less than 0.72 pK_a unit (our previous study[23] on 29 amines incorporating the Tissandier value of the proton hydration free energy achieved an AAD of 0.73 pK_a units at 298.15 K). This is equivalent to an absolute error of ≈ 4 kJ in the reaction free energy at 298.15 K, which is within so-called "chemical accuracy" of 1 kcal·mol^{-1}.

Our approach can be viewed as a methodology for accurately "bootstrapping" knowledge of the single well-studied MEA pK_a data point at 298.15 K to predict pK_a data both for MEA at higher temperatures and for other amines at all temperatures, requiring only the calculation of the reaction ideal–gas values and their solvation free energies.

Whereas the predicted pK_a values compare well with the experimental data, the intrinsic uncertainties in the experimental pK_c determinations complicate the direct comparison of such data with simulation values. However, we showed that our simulations of pK_c agree well with the scarcely available experimental data taking into account their mutual uncertainty; moreover, the molecular models are able to capture the trend in the carbamate formation

and the effect of steric hindrance on the pK_c.

We have provided temperature–dependent functions for the protonation and carbamate formation constants of the studied amines based on our methodology. These determine the corresponding standard reaction enthalpies as functions of temperature. Based on the same approach as followed in our recent purely predictive study for a set of 7 primary amines,[21] the simulation data/methodology provided here can be combined with the readily available experimental equilibrium constant data of the CO_2-H_2O binary system to give improved predictions for the speciation and equilibrium CO_2 loading of CO_2 in aqueous amine solutions.

In future work, equilibrium compositions calculated from our equilibrium constant predictions may be used in conjunction with the individual reaction enthalpies obtained in this work to predict both integral and differential overall heat (physical absorption + chemical reaction) of CO_2 absorption in the amine-water system, which is a fundamentally important quantity for solvent selection in the PCC process. For such calculations, isocoulombic reactions have the intrinsic advantage that the ionic activity coefficient contributions to the reaction free energy change cancel for simple models such as the Davies extension of the Debye-Hückel model, which become numerically equivalent to an ideal solution model.

Finally, the new H_3O^+ force field allows us to predict the solvation free energy of the proton, H^+, as a function of temperature. This provided a validation of the force field by showing that the proton solvation free energy at 298.15 K agrees well with the literature value. Furthermore, our calculations of the intrinsic proton solvation free energy can in principle be combined with temperature–dependent calculations of the Galvani potential to determine its absolute value as a function of temperature. This would enable the estimation of standard chemical potential and enthalpy data for all the ionic species considered in this study, which would be useful in the application of macroscopic thermodynamic models of aqueous solutions containing them.

6 Acknowledgements

Financial support was provided by the Natural Science and Engineering Council of Canada (NSERC) and the Agence Nationale de la Recherche (ANR) through the International Collaborative Strategic program between Canada and France (Grant NSERC STPGP 479466-15 and ANR-12-IS09-0001-01). We thank our industrial partner, Dr. John Carroll, Gas Liquids Engineering Ltd., for supporting this research and for helpful advice and encouragement. Computational facilities of the SHARCNET (Shared Hierarchical Academic Research Computing Network) HPC consortium (www.sharcnet.ca) and Compute Canada (www.computecanada.ca) are gratefully acknowledged.

Associated Content

The Supporting Information provides (1) coefficients for the temperature-dependent functions fitted to the dimensionless individual species infinite dilution chemical potentials $\frac{\mu_i^{res,\infty}}{RT}$, the protonation (R1) and carbamate formation reaction (R2) value of $\frac{\Delta G^0(T,p^0)}{RT}$, equilibrium constants, $\ln K$ and the reaction enthalpies of reactions R1 (ΔH^{deprot}) and R2 (ΔH^{carb}).(2) The GROMACS formatted force field parameters of all species.

Data and Software Availability

We used freely available Gromacs version 5.1.4 (https://www.gromacs.org/) for all MD simulations with the machine readable input files for all species provided in the Supplementary Information.

References

(1) Nielsen, C. J.; Herrmann, H.; Weller, C. Atmospheric chemistry and environmental impact of the use of amines in carbon capture and storage (CCS). *Chemical Society Reviews* **2012**, *41*, 6684–6704.

(2) Rochelle, G. T. Amine scrubbing for CO2 capture. *Science* **2009**, *325*, 1652–1654.

(3) Sartori, G.; Savage, D. W. Sterically hindered amines for carbon dioxide removal from gases. *Ind. & Eng. Chem. Fundam.* **1983**, *22*, 239–249.

(4) Fernandes, D.; Conway, W.; Burns, R.; Lawrance, G.; Maeder, M.; Puxty, G. Investigations of primary and secondary amine carbamate stability by 1H NMR spectroscopy for post combustion capture of carbon dioxide. *J. Chem. Thermodynamics* **2012**, *54*, 183–191.

(5) Aroua, M. K.; Benamor, A.; Haji-Sulaiman, M. Z. Equilibrium Constant for Carbamate Formation from Monoethanolamine and Its Relationship with Temperature. *J. Chem. Eng. Data* **1999**, *44*, 887–891.

(6) Hamborg, E. S.; Versteeg, G. F. Dissociation constants and thermodynamic properties of amines and alkanolamines from (293 to 353) K. *Journal of Chemical & Engineering Data* **2009**, *54*, 1318–1328.

(7) Simond, M. R.; Ballerat-Busserolles, K.; Coulier, Y.; Rodier, L.; Coxam, J.-Y. Dissociation Constants of Protonated Amines in Water at temperatures from 293.15 K to 343.15 K. *Journal of Solution Chemistry* **2012**, *41*, 130–142.

(8) Fernandes, D.; Conway, W.; Wang, X.; Burns, R.; Lawrance, G.; Maeder, M.; Puxty, G. Protonation constants and thermodynamic properties of amines for post combustion capture of CO2. *The Journal of Chemical Thermodynamics* **2012**, *51*, 97–102.

(9) McCann, N.; Maeder, M.; Hasse, H. A calorimetric study of carbamate formation. *The Journal of Chemical Thermodynamics* **2011**, *43*, 664–669.

(10) Jakobsen, J. P.; Krane, J.; Svendsen, H. F. Liquid-phase composition determination in CO2- H2O- alkanolamine systems: An NMR study. *Industrial & engineering chemistry research* **2005**, *44*, 9894–9903.

(11) Ciftja, A. F.; Hartono, A.; Svendsen, H. F. Experimental study on carbamate formation in the AMP–CO2–H2O system at different temperatures. *Chem. Eng. Sci.* **2014**, *107*, 317–327.

(12) Matin, N. S.; Remias, J. E.; Neathery, J. K.; Liu, K. Facile method for determination of amine speciation in CO2 capture solutions. *Industrial & engineering chemistry research* **2012**, *51*, 6613–6618.

(13) Ho, J.; Coote, M. L. A universal approach for continuum solvent p K a calculations: are we there yet? *Theoretical Chemistry Accounts* **2010**, *125*, 3–21.

(14) Xu, L.; Coote, M. L. Improving the accuracy of PCM-UAHF and PCM-UAKS calculations using optimized electrostatic scaling factors. *Journal of chemical theory and computation* **2019**, *15*, 6958–6967.

(15) Haworth, N. L.; Wang, Q.; Coote, M. L. Modeling flexible molecules in solution: A pKa Case Study. *J. Phys. Chem. A* **2017**, *121*, 5217–5225.

(16) da Silva, E. F.; Svendsen, H. F. Study of the carbamate stability of amines using ab initio methods and free-energy perturbations. *Industrial & engineering chemistry research* **2006**, *45*, 2497–2504.

(17) Pliego Jr, J. R. Thermodynamic cycles and the calculation of pKa. *Chemical physics letters* **2003**, *367*, 145–149.

(18) Miguel, E. L.; Silva, P. L.; Pliego, J. R. Theoretical prediction of pKa in methanol: Testing SM8 and SMD models for carboxylic acids, phenols, and amines. *J. Phys. Chem. B* **2014**, *118*, 5730–5739.

(19) Sakti, A. W.; Nishimura, Y.; Nakai, H. Rigorous p K a Estimation of Amine Species Using Density-Functional Tight-Binding-Based Metadynamics Simulations. *Journal of chemical theory and computation* **2018**, *14*, 351–356.

(20) Tummanapelli, A. K.; Vasudevan, S. Estimating successive p K a values of polyprotic acids from ab initio molecular dynamics using metadynamics: the dissociation of phthalic acid and its isomers. *Physical Chemistry Chemical Physics* **2015**, *17*, 6383–6388.

(21) Noroozi, J.; Smith, W. R. Accurately Predicting CO2 Reactive Absorption Properties in Aqueous Alkanolamine Solutions by Molecular Simulation Requiring No Solvent Experimental Data. *Industrial & Engineering Chemistry Research* **2020**, *59*, 18254–18268.

(22) Miron, G. D.; Kulik, D. A.; Thoenen, T. Generating isocoulombic reactions as a tool for systematic evaluation of temperature trends of thermodynamic properties: Application to aquocomplexes of lanthanides and actinides. *Geochimica et Cosmochimica Acta* **2020**, *286*, 119–142.

(23) Noroozi, J.; Smith, W. R. Prediction of Alkanolamine pKa Values by Combined Molecular Dynamics Free Energy Simulations and ab Initio Calculations. *Journal of Chemical & Engineering Data* **2019**,

(24) Tissandier, M. D.; Cowen, K. A.; Feng, W. Y.; Gundlach, E.; Cohen, M. H.; Earhart, A. D.; Coe, J. V.; Tuttle, T. R. The Proton's Absolute Aqueous Enthalpy and Gibbs Free Energy of Solvation from Cluster–Ion Solvation Data. *J. Phys. Chem. A* **1998**, *102*, 7787–7794.

(25) Noroozi, J.; Smith, W. R. An efficient molecular simulation methodology for chemical reaction equilibria in electrolyte solutions: Application to CO_2 reactive absorption. *The Journal of Physical Chemistry A* **2019**, *123*, 4074–4086.

(26) Malloum, A.; Fifen, J. J.; Conradie, J. Determination of the absolute solvation free energy and enthalpy of the proton in solutions. *J. Molecular Liquids* **2021**, *322*, 114919.

(27) Wang, J.; Wolf, R. M.; Caldwell, J. W.; Kollman, P. A.; Case, D. A. Development and Testing of a General Amber Force Field. *J. Comput. Chem.* **2001**, *25*, 1157–1174.

(28) Wang, J.; Wang, W.; Kollman, P. A.; Case, D. A. Automatic atom type and bond type perception in molecular mechanical calculations. *Journal of molecular graphics and modelling* **2006**, *25*, 247–260.

(29) Potoff, J. J.; Siepmann, J. I. Vapor-Liquid Equilibria of Mixtures Containing Alkanes, Carbon Dioxide, and Nitrogen. *AIChE J.* **2001**, *47*, 1676–1682.

(30) Bayly, C. I.; Cieplak, P.; Cornell, W.; Kollman, P. A. A well-behaved electrostatic potential based method using charge restraints for deriving atomic charges: the RESP model. *J. Phys. Chem.* **1993**, *97*, 10269–10280.

(31) da Silva, A. W. S.; Vranken, W. F. ACPYPE-Antechamber python parser interface. *BMC research notes* **2012**, *5*, 367.

(32) Martinez, L.; Andrade, R.; Birgin, E. G.; Martinez, J. M. PACKMOL: a package for building initial configurations for molecular dynamics simulations. *J Comput Chem* **2009**, *30*, 2157–2164.

(33) Pronk, S.; Pall, S.; Schulz, R.; Larsson, P.; Bjelkmar, P.; Apostolov, R.; Shirts, M. R.; Smith, J. C.; Kasson, P. M.; van der Spoel, D.; Hess, B.; Lindahl, E. GROMACS 4.5: a high–throughput and highly parallel open source molecular simulation toolkit. *Bioinformatics* **2013**, *29*, 845–854.

(34) Beutler, T. C.; Mark, A. E.; van Schaik, R. C.; Gerber, P. R.; Van Gunsteren, W. F. Avoiding singularities and numerical instabilities in free energy calculations based on molecular simulations. *Chem. Phys. Lett* **1994**, *222*, 529–539.

(35) Hatefi, N.; Smith, W. R. Ideal-Gas Thermochemical Properties for Alkanolamine and Related Species Involved in Carbon-Capture Applications. *J. Chem. Eng. Data* **2021**, *66*, 1592–1599.

(36) Rayer, A. V.; Sumon, K. Z.; Jaffari, L.; Henni, A. Dissociation constants (p K a) of tertiary and cyclic amines: Structural and temperature dependences. *Journal of Chemical & Engineering Data* **2014**, *59*, 3805–3813.

(37) Tagiuri, A.; Mohamedali, M.; Henni, A. Dissociation constant (p K a) and thermodynamic properties of some tertiary and cyclic amines from (298 to 333) K. *Journal of Chemical & Engineering Data* **2016**, *61*, 247–254.

(38) Kim, I.; Jens, C. M.; Grimstvedt, A.; Svendsen, H. F. Thermodynamics of protonation of amines in aqueous solutions at elevated temperatures. *The Journal of Chemical Thermodynamics* **2011**, *43*, 1754–1762.

(39) Littel, R. J.; Bos, M.; Knoop, G. J. Dissociation constants of some alkanolamines at 293, 303, 318, and 333 K. *Journal of chemical and engineering data* **1990**, *35*, 276–277.

(40) Oscarson, J.; Wu, G.; Faux, P.; Izatt, R.; Christensen, J. Thermodynamics of protonation of alkanolamines in aqueous solution to 325 C. *Thermochimica acta* **1989**, *154*, 119–127.

(41) Bates, R. G.; Pinching, G. D. Acidic dissociation constant and related thermodynamic quantities for monoethanolammonium ion in water from 0 to 50 C. *Journal of Research of the National Bureau of Standards* **1951**, *46*, 349352.

(42) Puxty, G.; Rowland, R.; Allport, A.; Yang, Q.; Bown, M.; Burns, R.; Maeder, M.; Attalla, M. Carbon dioxide postcombustion capture: a novel screening study of the carbon dioxide absorption performance of 76 amines. *Env. Sci. & Technology* **2009**, *43*, 6427–6433.

(43) Fernandes, D.; Conway, W.; Wang, X.; Burns, R.; Lawrance, G.; Maeder, M.; Puxty, G. Protonation constants and thermodynamic properties of amines for post combustion capture of CO2. *The Journal of Chemical Thermodynamics* **2012**, *51*, 97–102.

(44) Conway, W.; Wang, X.; Fernandes, D.; Burns, R.; Lawrance, G.; Puxty, G.; Maeder, M. Toward the understanding of chemical absorption processes for post-combustion capture of carbon dioxide: electronic and steric considerations from the kinetics of reactions of $CO_2$2 (aq) with sterically hindered amines. *Env. Sci. & Technology* **2013**, *47*, 1163–1169.

(45) Böttinger, W.; Maiwald, M.; Hasse, H. Online NMR spectroscopic study of species distribution in MEA–H2O–CO2 and DEA–H2O–CO2. *Fluid Phase Equilibria* **2008**, *263*, 131–143.

(46) Austgen, D. M.; Rochelle, G. T.; Peng, X.; Chen, C. C. Model of Vapor Liquid Equilibria for Aqueous Acid Gas Alkanolamine Systems Using the Electrolyte NRTL Equation. *Ind. Eng. Chem. Res.* **1989**, *28*, 1060–1073.

(47) Fennell, C. J.; Wymer, K. L.; Mobley, D. L. A fixed-charge model for alcohol polarization in the condensed phase, and its role in small molecule hydration. *J Phys Chem B* **2014**, *118*, 6438–46.

(48) Fernandes, D.; Conway, W.; Wang, X.; Burns, R.; Lawrance, G.; Maeder, M.; Puxty, G. Protonation constants and thermodynamic properties of amines for post combustion capture of CO_2. *J. Chem. Thermodynamics* **2012**, *51*, 97–102.

(49) Datta, S.; Grzybowski, A. 593. Acid dissociation constants of the ammonium group in 2-aminoethanol, 2-aminoethyl phosphate, and 2-aminoethyl sulphate. *Journal of the Chemical Society (Resumed)* **1962**, 3068–3077.

(50) Timimi, B.; Everett, D. The thermodynamics of the acid dissociation of some amino-alcohols in water. *Journal of the Chemical Society B: Physical Organic* **1968**, 1380–1386.

(51) Hetzer, H. B.; Bates, R. G. DISSOCIATION CONSTANT OF 2-AMMONIUM-2-METHYL-1, 3-PROPANEDIOL IN WATER FROM 0 TO 50 AND RELATED THERMODYNAMIC QUANTITIES. *The Journal of Physical Chemistry* **1962**, *66*, 308–311.

(52) Bower, V. E.; Robinson, R. A.; Bates, R. G. Acidic dissociation constant and related thermodynamic quantities for diethanolammonium ion in water from 0 to 50 C. *J. Res. Natl. Bur. Stand. A* **1962**, *66*, 71–75.

(53) Kim, J.-H.; Dobrogowska, C.; Hepler, L. G. Thermodynamics of ionization of aqueous alkanolamines. *Canadian journal of chemistry* **1987**, *65*, 1726–1728.

(54) Xu, S.; Wang, Y.; Otto, F. D.; Mather, A. E. Physicochemical properties of 2-piperidineethanol and its aqueous solutions. *Journal of Chemical and Engineering Data* **1992**, *37*, 407–411.

(55) Jou, F.-Y.; Mather, A. E.; Otto, F. D. The solubility of CO2 in a 30 mass percent monoethanolamine solution. *Can. J. Chem. Eng.* **1995**, *73*, 140–147.

(56) Park, S. H.; Lee, K. B.; Hyun, J. C.; Kim, S. H. Correlation and prediction of the solubility of carbon dioxide in aqueous alkanolamine and mixed alkanolamine solutions. *Industrial & engineering chemistry research* **2002**, *41*, 1658–1665.

(57) Malhotra, D.; Cantu, D. C.; Koech, P. K.; Heldebrant, D. J.; Karkamkar, A.; Zheng, F.; Bearden, M. D.; Rousseau, R.; Glezakou, V.-A. Directed Hydrogen Bond Placement:

Low Viscosity Amine Solvents for CO2 Capture. *ACS Sustainable Chemistry & Engineering* **2019**, *7*, 7535–7542.

(58) Jensen, M. B.; Jorgensen, E.; Faurholt, C. Reactions between Carbon Dioxide and Amino Alcohols. 1. Monoethanolamine and Diethanolamine. *Acta Chemica Scandinavica* **1954**, *8*, 1137–1140.

(59) Vácha, R.; Buch, V.; Milet, A.; Devlin, J. P.; Jungwirth, P. Autoionization at the surface of neat water: is the top layer pH neutral, basic, or acidic? *Physical Chemistry Chemical Physics* **2007**, *9*, 4736–4747.

(60) Hunter, E. P.; Lias, S. G. Evaluated gas phase basicities and proton affinities of molecules: an update. *J. Phys. Chem. Ref. Data* **1998**, *27*, 413–656.

(61) Linstrom, P. J.; Mallard, W. G. The NIST Chemistry WebBook: A chemical data resource on the internet. *Journal of Chemical & Engineering Data* **2001**, *46*, 1059–1063.

(62) Palascak, M. W.; Shields, G. C. Accurate experimental values for the free energies of hydration of H+, OH-, and H3O+. *The Journal of Physical Chemistry A* **2004**, *108*, 3692–3694.

(63) Zhan, C.-G.; Dixon, D. A. Absolute hydration free energy of the proton from first-principles electronic structure calculations. *The Journal of Physical Chemistry A* **2001**, *105*, 11534–11540.

(64) Camaioni, D. M.; Schwerdtfeger, C. A. Comment on Accurate experimental values for the free energies of hydration of H+, OH-, and H3O+. *The Journal of Physical Chemistry A* **2005**, *109*, 10795–10797.

(65) Zhang, H.; Jiang, Y.; Yan, H.; Yin, C.; Tan, T.; van der Spoel, D. Free-energy calcula-

tions of ionic hydration consistent with the experimental hydration free energy of the proton. *J. Phys. Chem. Lett.* **2017**, *8*, 2705–2712.

(66) Lamoureux, G.; Roux, B. Absolute hydration free energy scale for alkali and halide ions established from simulations with a polarizable force field. *J. Phys. Chem. B* **2006**, *110*, 3308–3322.